



1 **Spatiotemporal variability and contribution of different aerosol**
2 **types to the Aerosol Optical Depth over the Eastern Mediterranean**

3
4 **Aristeidis K. Georgoulas^{1,2,3,*}, Georgia Alexandri^{4,5}, Konstantinos A. Kourtidis⁵,**
5 **Jos Lelieveld^{3,6}, Prodromos Zanis¹, Ulrich Pöschl², Robert Levy⁷, Vassilis**
6 **Amiridis⁸, Eleni Marinou^{4,8}, Athanasios Tsikerdekis¹**

7
8 [1] Department of Meteorology and Climatology, School of Geology, Aristotle University of
9 Thessaloniki, 54124, Thessaloniki, Greece

10 [2] Multiphase Chemistry Department, Max Planck Institute for Chemistry, D-55128, Mainz,
11 Germany

12 [3] Energy, Environment and Water Research Center, The Cyprus Institute, Nicosia, Cyprus

13 [4] Laboratory of Atmospheric Physics, Physics Department, Aristotle University of
14 Thessaloniki, 54124, Thessaloniki, Greece

15 [5] Laboratory of Atmospheric Pollution and Pollution Control Engineering of Atmospheric
16 Pollutants, Department of Environmental Engineering, Democritus University of Thrace,
17 67100, Xanthi, Greece

18 [6] Atmospheric Chemistry Department, Max Planck Institute for Chemistry, D-55128,
19 Mainz, Germany

20 [7] Earth Science Division, NASA Goddard Space Flight Center, MD 20771, Greenbelt, USA

21 [8] Institute for Astronomy, Astrophysics, Space Application and Remote Sensing, National
22 Observatory of Athens, 15236 Athens, Greece

23 **current address: Laboratory of Atmospheric Pollution and Pollution Control Engineering of*
24 *Atmospheric Pollutants, Department of Environmental Engineering, Democritus University of*
25 *Thrace, 67100, Xanthi, Greece*

26
27 Correspondence to: A. K. Georgoulas (argeor@env.duth.gr)

28
29 **Abstract**

30 This study characterizes the spatiotemporal variability and relative contribution of different
31 types of aerosols to the Aerosol Optical Depth (AOD) over the Eastern Mediterranean as
32 derived from MODIS Terra (3/2000-12/2012) and Aqua (7/2002-12/2012) satellite
33 instruments. For this purpose, a 0.1° x 0.1° gridded MODIS dataset was compiled and



1 validated against AERONET sunphotometric observations. The high spatial resolution and
2 long temporal coverage of the dataset allows for the determination of local hot spots like
3 megacities, medium sized cities, industrial zones, and power plant complexes, seasonal
4 variabilities, and decadal averages. The average AOD at 550 nm (AOD_{550}) for the entire
5 region is $\sim 0.22 \pm 0.19$ with maximum values in summer and seasonal variabilities that can be
6 attributed to precipitation, photochemical production of secondary organic aerosols, transport
7 of pollution and smoke from biomass burning in Central and Eastern Europe, and transport of
8 dust from the Sahara Desert and the Middle East. The MODIS data were analyzed together
9 with data from other satellite sensors, reanalysis projects and a chemistry-aerosol-transport
10 model using an optimized algorithm tailored for the region and capable of estimating the
11 contribution of different aerosol types to the total AOD_{550} . The spatial and temporal
12 variability of anthropogenic, dust and fine mode natural aerosols over land and anthropogenic,
13 dust and marine aerosols over the sea is examined. The relative contribution of the different
14 aerosol types to the total AOD_{550} exhibits a low/high seasonal variability over land/oceanic
15 areas, respectively. Overall, anthropogenic aerosols, dust and fine mode natural aerosols
16 account for $\sim 51\%$, $\sim 34\%$ and $\sim 15\%$ of the total AOD_{550} over land, while, anthropogenic
17 aerosols, dust and marine aerosols account $\sim 40\%$, $\sim 34\%$ and $\sim 26\%$ of the total AOD_{550}
18 over the sea, based on MODIS Terra and Aqua observations.

19

20 **1 Introduction**

21 For more than fifteen years, two MODIS (Moderate Resolution Imaging Spectroradiometer)
22 satellite sensors monitor tropospheric aerosols at a global scale on a daily basis. The retrieved
23 aerosol optical properties have been used in numerous air quality studies as well as studies
24 related to the effect of airborne particles on various climatic parameters (e.g. radiation, clouds,
25 precipitation, etc.). The $1^\circ \times 1^\circ$ daily gridded level-3 dataset is primarily used for global as well
26 as regional studies while the single pixel level-2 data with a 10 km resolution (at nadir) are
27 mostly used for regional and local scale studies. Nevertheless, the use of the coarse resolution
28 MODIS data has predominated even in regional studies. The reasons for this could be the
29 smaller file size which makes their processing and storage easier or the fact that they are easily
30 accessible through user-friendly data bases which also allow for a very basic analysis like e.g.
31 NASA's GIOVANNI website (<http://giovanni.gsfc.nasa.gov/giovanni/>) (Acker and Leptoukh,
32 2007).



1 The same holds for studies focusing on the Mediterranean Basin, an area which is considered of
2 particular sensitivity as far as air pollution and climate change is concerned (Lelieveld et al.,
3 2002, Giorgi, 2006). The Mediterranean basin is one of the regions with highest aerosol optical
4 depths (AODs) in the world (Husar et al., 1997; Ichocku et al., 2005; Papadimas et al., 2008),
5 causing significant climate forcing especially in summer, which is characterized by low
6 cloudiness and high incoming solar radiation levels (Papadimas et al., 2012; Alexandri et al.,
7 2015). The Mediterranean is also recognized as a crossroads between three continents where
8 aerosols of various types accumulate. Marine aerosols from the Mediterranean Sea and even the
9 Atlantic Ocean combine with aerosols from continental Europe (urban and rural), dust particles
10 transported from the Sahara Desert and Middle East as well as biomass burning aerosols from
11 occasional wild fires and agricultural burning (Lelieveld et al., 2002). Specifically, as discussed
12 in Hatzianastassiou et al. (2009), the Eastern Mediterranean, the region under investigation here,
13 is located at a "key" point of this crossroads. There is a significant number of ground and
14 satellite-based studies on the abundance and optical properties of tropospheric aerosols in the
15 area; however, these studies are either focused on specific spots or applied a coarse spatial and
16 temporal resolution.

17 The ground-based instrumentation used in studies focusing on the aerosol load and optical
18 properties over the Eastern Mediterranean includes active and passive sensors such as Lidars
19 (e.g. Papayannis and Balis, 1998; Balis et al., 2004; Papayannis et al., 2005, 2009; Amiridis et
20 al., 2005, 2009; Mamouri et al., 2013; Kokkalis et al., 2013; Nisantzi et al., 2015), Cimel
21 sunphotometers (e.g. Israelevich et al., 2003; Kubilay et al., 2003; Derimian et al., 2006;
22 Kalivitis et al., 2007; Kelektsoğlu and Rapsomanikis, 2011; Nikitidou and Kazantzidis, 2013),
23 Brewer spectrophotometers (e.g. Kazadzis et al., 2007; Koukouli et al., 2010), Multi-Filter
24 Radiometers (e.g. Gerasopoulos et al., 2009, 2011; Kazadzis et al., 2014), ceilometers (e.g.
25 Tsaknakis et al., 2011), Microtops sunphotometers (e.g. El-Metwally and Alfaro al., 2013), etc.
26 However, these and other studies not referenced here either refer to specific spots with the
27 majority of the ground stations being situated in large urban centers (e.g. Athens, Thessaloniki,
28 Cairo) or to specific events (e.g. Sahara dust intrusions, biomass burning events, etc.).

29 On the other hand, AOD and other aerosol optical properties have been studied over the greater
30 Eastern Mediterranean region based on data from Meteosat (Moulin et al., 1998), SeaWiFS
31 (Koren et al., 2003; Antoine and Nobileau, 2006; Mélin et al., 2007; Nabat et al., 2013), TOMS
32 (Alpert and Ganor, 2001; Israelevich et al., 2002; Koukouli et al. 2006; Hatzianastassiou et al.,
33 2009; Koukouli et al., 2010, Israelevich et al., 2012, Kaskaoutis et al., 2012a; Nabat et al., 2013;



1 Gkikas et al., 2013; 2014; Varga et al., 2014), MODIS Terra and Aqua (Barnaba and Gobbi,
2 2004; Papayannis et al., 2005; Kaskaoutis et al., 2007; 2008; 2010; 2011; 2012a,b,c,d;
3 Kosmopoulos et al., 2008; Papadimas et al., 2008, 2009; Rudich et al., 2008; Carmona and
4 Alpert, 2009; Karnieli et al., 2009; Gkikas et al., 2009; 2013; Hatzianastassiou et al., 2009; El-
5 Metwally et al., 2010; Koukouli et al., 2010; Kanakidou et al., 2011; Gerasopoulos et al., 2011;
6 de Meij and Lelieveld, 2011; Marey et al., 2011; de Meij et al., 2012; Nabat et al., 2012, 2013;
7 Nikitidou and Kazantzidis, 2013; Athanasiou et al., 2013; Benas et al., 2011; 2013; Sorek-
8 Hamer et al., 2013; Kabatas et al., 2014; Kourtidis et al., 2014; Mishra et al., 2014; Flaounas et
9 al., 2015; Kloog et al., 2015), OMI/AURA (Kaskaoutis et al., 2010; El-Metwally et al., 2010;
10 Marey et al., 2011; Kaskaoutis et al., 2012b,c, Gkikas et al., 2013; 2014; Sorek-Hamer et al.,
11 2013; Varga et al., 2014; Flaounas et al., 2015), CALIOP/CALIPSO (Amiridis et al., 2009,
12 2013, Mamouri et al., 2009; Marey et al., 2011; Kaskaoutis et al., 2012c; de Meij et al., 2012;
13 Nabat et al., 2012, 2013; Mamouri and Ansmann, 2015), MISR/Terra (Kanakidou et al., 2011;
14 Marey et al., 2011; de Meij and Lelieveld, 2011; de Meij et al., 2012; Nabat et al., 2013;
15 Kabatas et al., 2014; Abdelkader et al., 2015) as well as NOAA/AVHRR, MERIS/ENVISAT,
16 AATSR/ENVISAT, PARASOL/POLDER, MSG/SEVIRI, and Landsat satellite data (see
17 Retalis and Sifakis, 2010; Nabat et al., 2013; Benas et al., 2013; Sifakis et al., 2014). To our
18 knowledge, these studies comprise the majority of work focusing on tropospheric aerosols over
19 the Eastern Mediterranean by means of satellite remote sensing, published in peer reviewed
20 journals the last ~ 15 years. As shown in Fig. 4 of this work, the publication rate of satellite-
21 based studies focusing on Eastern Mediterranean aerosols nearly doubled every three years
22 during the period 1997-2014 which is indicative of the increasing scientific interest in the area.
23 In a very large fraction of the satellite-based studies referenced above, the used data are either of
24 coarse mode (usually 1° which is ~ 100 km for the mid-latitudes) or focus on specific spots for
25 validation purposes. In a few cases, high resolution data were used in spatiotemporal studies;
26 however, either these studies are restricted over surfaces covered by water or examine a short
27 period only. For example, Moulin et al. (1998) investigated the dust AOD patterns over the
28 oceanic areas of the Mediterranean Basin at a resolution of $35 \times 35 \text{ km}^2$ for a period of 11 years
29 (1984-1994) using Meteosat observations. A 7-year climatology (1998-2004) of total and dust
30 AOD for the same regions at a resolution of $0.16^\circ \times 0.16^\circ$ was compiled by Antoine and
31 Nobileau (2006) using observations from SeaWIFS. Mélin et al. (2007) merged SeaWIFS and
32 MODIS data and presented high resolution AOD patterns ($2 \times 2 \text{ km}^2$) for May 2003. As far as
33 MODIS is concerned, only Barnaba and Gobbi (2004) presented a high resolution ($0.1^\circ \times 0.1^\circ$)



1 spatiotemporal analysis for a period of 1 year (2001) over ocean only. In a recent paper,
2 Athanasiou et al. (2013) presented in detail a method for compiling a 0.5-degree resolution
3 AOD gridded dataset using level-2 MODIS Terra data for the greater region of Greece (2000-
4 2008). However, the spatial resolution they used (~ 50 km) is not high enough to reveal local
5 sources (e.g. cities, islands, river banks, etc.). Overall, there has not been so far any detailed
6 high resolution spatiotemporal study of the AOD over Eastern Mediterranean.

7 In this paper, the AOD₅₅₀ spatiotemporal variability over the Eastern Mediterranean (30°N-
8 45°N, 17.5°E-37.5°E) is presented at a high spatial resolution (0.1° x 0.1°) based on MODIS
9 Terra and Aqua observations. Level-2 MODIS data are used for the compilation of a 0.1-degree
10 gridded dataset which is validated against ground-based observations. In order to calculate the
11 contribution of different aerosol types to the total AOD, the MODIS data were analyzed
12 together with other satellite data, ERA-Interim reanalysis data and the Goddard Chemistry
13 Aerosol Radiation and Transport (GOCART) model using an algorithm optimized for the
14 surface properties of the Eastern Mediterranean region. The different datasets used in this
15 research are presented in detail in Sect. 2 while a detailed description of the method is given in
16 Sect. 3. Sect. 4 includes the results from the MODIS validation procedure, the annual and
17 seasonal variability of AOD₅₅₀ over the region with a discussion on the local aerosol sources
18 and the differences between Terra and Aqua, and the annual and seasonal contribution of
19 different aerosol types to the total AOD₅₅₀. Finally, in Sect. 5, the main conclusions of the paper
20 are presented along with a short discussion on how these results could contribute to future
21 studies in the area.

22

23 **2 Observations, reanalysis data and model simulations**

24 **2.1 MODIS Terra and Aqua satellite observations**

25 The main data used in this work come from the level-2 MODIS Terra (MOD04_L2) and
26 MODIS Aqua (MYD04_L2) Collection 051 dataset and have been acquired through NASA's
27 Level 1 and Atmosphere Archive and Distribution System (LAADS)
28 (<http://ladsweb.nascom.nasa.gov>). The fact that MODIS Terra and Aqua have a daytime
29 equator crossing time at 10:30 LT (morning) and 13:30 LT (noon), respectively. MODIS
30 instruments with a viewing swath of 2330 km measure backscattered radiation at 36 spectral
31 bands between 0.415 and 14.235 μm with a spatial resolution of 250, 500 and 1000 m,
32 providing a nearly global coverage on a daily basis. Aerosol optical properties for the
33 standard MODIS aerosol product are retrieved using two different "Dark Target" (DT)



1 algorithms. The one is used over land surfaces (Kaufman et al., 1997; Levy et al., 2007a, b;
2 Remer et al., 2005; Levy et al., 2010) and the other over oceanic regions (Tanré et al., 1997;
3 Levy et al., 2003; Remer et al., 2005). The "Deep Blue" algorithm (DB) (Hsu et al., 2004;
4 Hsu et al., 2006) has been used for retrievals over bright land surfaces (e.g. deserts) where the
5 DT algorithm fails. Only recently, updates to the algorithm allowed for extending the spatial
6 coverage of the DB aerosol product over all land areas (Hsu et al., 2013; Sayer et al., 2013;
7 2014). AERONET Cimel sunphotometric measurements have been extensively used for the
8 validation of the MODIS over-land and over-ocean products (e.g. Chu et al., 2002; Remer et
9 al., 2002; Remer et al., 2005; Levy et al., 2010; Shi et al., 2013).

10 In this work, AOD₅₅₀ over both land and ocean and the Fine Mode Ratio (FMR₅₅₀) over ocean
11 from Collection 051 were used at a spatial resolution of 10 km (at nadir). The uncertainty of
12 the MODIS aerosol optical depth has been estimated at $\pm(0.05+0.15AOD)$ over land (Chu et
13 al., 2002; Levy et al., 2010) and $\pm(0.03+0.05AOD)$ over ocean (Remer et al., 2002) relative to
14 the AERONET AOD. Specifically, for the DT data used in this work only high quality
15 retrievals are used over land. This means that the data have a Quality Assurance Confidence
16 (QAC) flag equal to 3 (high confidence). For retrievals over ocean we use data with a QAC
17 flag of 1 (marginally good), 2 (good) and 3 (see Levy et al., 2009 for details). The pre-launch
18 uncertainty of FMR₅₅₀ is $\pm 30\%$ over ocean (Remer et al., 2005) while over land this
19 parameter is by no means trustworthy and should only be used in qualitative studies (e.g. see
20 Georgoulias and Kourtidis, 2011). In cases where DT algorithm does not provide products
21 over land, especially over bright arid and semi-arid regions of North Africa, AOD₅₅₀ values
22 from the DB algorithm are used in our work. The expected uncertainty of the DB product
23 used here is $\pm(0.05+0.2AOD)$ relative to the AERONET AOD (Hsu et al., 2006). The
24 analyzed datasets cover the period from 3/2000 to 12/2012 for Terra and from 7/2002 to
25 12/2012 for Aqua MODIS covering the region of Eastern Mediterranean. The Collection 051
26 DB data for Terra are available only until 12/2007 due to calibration issues; nevertheless,
27 these data are carefully used within our analysis to get a complete image of the aerosol load
28 over the region.

29

30 **2.2 AERONET ground-based observations**

31 For the evaluation of the MODIS AOD₅₅₀, data from 13 AERONET Cimel network ground
32 stations in the region of Eastern Mediterranean have been acquired
33 (<http://aeronet.gsfc.nasa.gov>). The stations were selected such as their operation period covers



1 at least 2 years and there are at least 100 common days of co-localized AERONET and
2 MODIS observations. AERONET Cimel sunphotometers measure solar radiation every 15
3 minutes within the spectral range from 340 to 1020 nm (Holben et al., 2001). The spectral
4 measurements allow for the retrieval of columnar aerosol properties (see Holben et al., 1998;
5 Dubovik and King, 2000; Dubovik et al., 2000, 2002). The AERONET AOD uncertainty is in
6 the order of 0.01-0.02 (Eck et al., 1999), being larger at shorter wavelengths. Here, we use
7 quadratic fits on a log-log scale to interpolate the AERONET data (AODs at 440, 500, 675
8 and 870 nm) to the MODIS band-effective wavelength of 550 nm (Eck et al., 1999; Levy et
9 al., 2010). Simultaneous measurements of the Ångström Exponent (AE) for the spectral range
10 440-870 nm (AE₄₄₀₋₈₇₀) from the 13 AERONET stations mentioned above were also
11 utilized in this work in order to account for days with dust dominance. The uncertainty of the
12 AE is significantly higher than the AOD uncertainty, especially under low-AOD conditions.
13 Li et al. (2014) found that the uncertainty for a typical Northern Hemispheric AERONET
14 station (GSFC) is ~ 0.6 during winter when AODs are significantly lower compared to
15 summer (~ 0.15).

16

17 **2.3 LIVAS CALIOP/CALIPSO dust climatology**

18 Dust aerosol optical depths at 532 nm (AOD₅₃₂) from CALIOP/CALIPSO (Cloud-Aerosol
19 Lidar with Orthogonal Polarization instrument aboard Cloud-Aerosol Lidar and Infrared
20 Pathfinder Satellite Observations satellite) at a resolution of $1^\circ \times 1^\circ$ are also used here for the
21 period 2007-2012. CALIPSO measures cloud and aerosol properties flying at a 705 km sun
22 synchronous polar orbit with a 16 day repeat cycle and an equator-crossing time close to that
23 of the Aqua satellite (13:30 LT). The dust product used here comes from a Saharan-dust-
24 optimized retrieval scheme that was developed within the framework of the LIVAS (Lidar
25 Climatology of Vertical Aerosol Structure for Space-Based LIDAR Simulation Studies)
26 project (Amiridis et al. 2015) and has been presented in detail in Amiridis et al. (2013). In
27 brief, the LIVAS dust product is optimized for Europe by using a lidar ratio of 58 sr instead of
28 40 sr is applied to Level 2 dust related backscatter products. This correction results to an
29 improved AOD₅₃₂ absolute bias of ~ -0.03 compared to spatially and temporally co-located
30 AERONET observations (Amiridis et al., 2013). The corresponding reported biases for the
31 original CALIPSO data are significantly higher (~ -0.10). The bias is even lower when
32 compared against MODIS satellite-based observations. Other improvements of this product
33 are related to the use of a new methodology for the calculation of pure dust extinction from



1 dust mixtures and the application of an averaging scheme that includes zero extinction values
2 for the non-dust aerosol types detected. Overall, this product (hereafter denoted as LIVAS
3 dust product) exhibits better agreement with observations from MODIS and AERONET and
4 simulations from the BSC-DREAM8b dust model over North Africa and Europe than the
5 standard CALIPSO data hence being an ideal tool for the evaluation of other satellite-based
6 products.

7

8 **2.4 Earth Probe TOMS and OMI satellite observations**

9 For this work, Aerosol Index (AI) data (Herman et al., 1997) from the Earth Probe TOMS
10 (Total Ozone Mapping) spectrometer aboard Earth Probe for the period 1/2000-9/2004 at a
11 resolution of $1^\circ \times 1.25^\circ$ and the OMI (Ozone Monitoring Instrument) sensor aboard EOS
12 AURA for the period 10/2004-12/2012 at a resolution of $1^\circ \times 1^\circ$ were acquired through the
13 GIOVANNI web database (<http://giovanni.gsfc.nasa.gov/giovanni/>). Earth Probe TOMS
14 continued the record of the first three TOMS instruments aboard Nimbus-7, Meteor-3 and
15 ADEOS flying in a sun synchronous orbit at an altitude of 740 km with an instantaneous field
16 of view size of $39 \times 39 \text{ km}^2$ at nadir. The instrument had an ascending node equator crossing
17 time at 12:00 LT covering 85 % of the globe on a daily basis from 7/1996 until 12/2005. The
18 satellite was originally set to a 500 km sun synchronous orbit but was set to its final orbit after
19 the failure of ADEOS satellite in 6/1997. OMI is a UV/VIS nadir solar backscatter
20 spectrometer (Levelt et al., 2006) that continues the long TOMS record. OMI flies in a sun
21 synchronous polar orbit at an altitude of 705 km with an ascending node equator crossing
22 time at 13:45 LT. Its 2600 km viewing swath allows for almost daily global coverage while
23 the spatial resolution of the instrument is $13 \times 24 \text{ km}^2$ at nadir. The AI which is calculated by
24 the two instruments constitutes a qualitative indicator of the presence of UV absorbing
25 aerosols in the atmosphere (e.g. biomass burning, dust). The Version 8 algorithm is applied on
26 spectral measurements from both TOMS and OMI sensor to produce a consistent long-term
27 AI timeseries (Li et al., 2009). AI is calculated from the difference in surface reflectivity
28 derived from the 331.2 and 360 nm measurements exhibiting an uncertainty of $\pm 30 \%$ (Torres
29 et al., 2007).

30

31 **2.5 ERA-Interim reanalysis data**

32 Wind speed (ws) data at 10 m above surface from the ERA-Interim reanalysis (Dee et al.,
33 2011) are used for 9:00 and 12:00 UTC on a daily basis for the period 2000-2012. We use



1 9:00 and 12:00 UTC data in order to be closer to the Terra and Aqua overpass time in the
2 area, respectively. The various ERA-Interim reanalysis fields are produced by ECMWF's
3 Integrated Forecast System (IFS) assimilating satellite and ground-based observations. The
4 system includes a 4-D variational analysis with a 12-hour analysis window. The spatial
5 resolution of the ERA-Interim data is ~ 79 km with 60 vertical levels from the surface up to
6 0.1 hPa while the data can be acquired at various resolutions through ECMWF's website
7 (<http://apps.ecmwf.int/datasets/data/interim-full-daily/>). Over ocean, the 10 m ERA-interim
8 wind speed exhibits a bias of less than -0.5 m/s compared to quality-controlled in situ
9 observations on a global scale (Dee et al., 2011). Specifically, for the region of Eastern
10 Mediterranean examined here, the 10 m ERA-interim wind speed exhibits a bias of -0.96 m/s
11 (-16%) compared to satellite-based observations from QuikSCAT (Hermann et al., 2011).

12

13 **2.6 MACC reanalysis data**

14 The daily MACC total and dust AOD₅₅₀ data for the period 2003-2012 come from the aerosol
15 analysis and forecast system of ECMWF which consists of a forward model (Morcrette et al.,
16 2009) and a data-assimilation module (Benedetti et al., 2009). AOD₅₅₀ measurements from
17 the two MODIS instruments aboard Terra and Aqua are assimilated by the MACC forecasting
18 system through a 4D-Var assimilation algorithm to produce the aerosol analysis, leading to an
19 improved AOD representation compared to observations (see Benedetti et al., 2009; Mangold
20 et al., 2011). Five aerosol species are included within MACC, namely, mineral dust, sea salt,
21 sulfates, black carbon and organic matter. Three different size bins are used for mineral dust
22 and sea salt particles while the black carbon and organic material are distributed to a
23 hydrophilic and a hydrophobic mode. Dust and sea salt emissions are given as a function of
24 surface wind speed, while the emissions of the other species are taken from inventories. The
25 spatial resolution of the MACC reanalysis data is ~ 79 km with 60 vertical levels from the
26 surface up to 0.1 hPa and can be acquired through: [http://apps.ecmwf.int/datasets/data/macc-](http://apps.ecmwf.int/datasets/data/macc-reanalysis/)
27 [reanalysis/](http://apps.ecmwf.int/datasets/data/macc-reanalysis/). The MACC total and dust AODs have been evaluated against ground and
28 satellite-based observations (see Elguindi et al., 2010; Bellouin et al., 2013; Inness et al.,
29 2013; Cesnulyte et al., 2014; Cuevas et al., 2015) showing that the MACC aerosol products
30 generally capture well the daily, seasonal and interannual variability of aerosols. As discussed
31 in Bellouin et al. (2013) the uncertainties of MACC total AOD₅₅₀ (~ 0.03) and dust AOD₅₅₀ (\sim
32 0.014) arise from uncertainties in the MODIS retrievals which are assimilated into the model
33 and errors in the forward modeling of total and component AODs.



1

2 **2.7 GOCART data**

3 Daily total and dust AOD₅₅₀ data from the GOCART chemistry-aerosol-transport model
4 simulations (version 006) are used in this study for the period 2000-2007. The GOCART
5 model (see Chin et al., 2000, 2002, 2004, 2007; Ginoux et al., 2001, 2004) uses the
6 assimilated meteorological fields of the Goddard Earth Observing System Data Assimilation
7 System (GEOS DAS) which are generated by the Goddard Global Modeling and Assimilation
8 Office (GMAO). The data which are used were acquired from an older version of NASA's
9 GIOVANNI web database (<http://disc.sci.gsfc.nasa.gov/giovanni/>) and come from a
10 simulation implemented at a spatial resolution of 2° (latitude) x 2.5° (longitude) with 30
11 vertical sigma layers (Chin et al., 2009). The model includes physicochemical processes of
12 major tropospheric aerosol components (sulfates, dust, black carbon, organic carbon, sea salt)
13 and precursor gases (SO₂ and dimethylsulfide) incorporating various atmospheric processes.
14 The total AOD₅₅₀ from GOCART compared to ground-based observations from the
15 AERONET exhibits a relative mean bias [mean(GOCART)/mean(AERONET)] of 1.120,
16 1.135 and 0.959 over Europe, North Africa and for the whole globe, respectively.

17

18 **2.8 Ancillary data**

19 Apart from the primary datasets presented above, three additional datasets were used in order
20 to support our findings. OMI/AURA daily gridded (Bucsela et al., 2013) tropospheric NO₂
21 columnar data (OMNO2d version 2.1) at a spatial resolution of 0.25° x 0.25° were acquired
22 from NASA's GIOVANNI web database (<http://giovanni.gsfc.nasa.gov/giovanni/>) for the
23 period 2005-2012. The quality checked data used in this work correspond to sky conditions
24 where cloud fraction is less than 30 %. Planetary boundary layer (PBL) SO₂ daily gridded
25 columnar data (OMSO2e version 1.1.7) were also acquired from GIOVANNI for the same
26 period. The OMSO2e gridded data (0.25° x 0.25°) used in this work are produced from best
27 level-2 pixel data, screened for OMI row anomaly and other data quality flags. The PBL SO₂
28 column retrievals are produced with an algorithm based on principal component analysis
29 (PCA) of the OMI radiance data (Li et al., 2013). Finally, monthly precipitation data from the
30 3B43 TRMM and Other Sources Monthly Rainfall Product (version 7) at a spatial resolution
31 of 0.25° x 0.25° for the period 2000-2012 were obtained from GIOVANNI. This dataset is
32 derived from 3-hourly precipitation retrievals from the Precipitation Radar (PR), the TRMM
33 Microwave Imager (TMI) and the Visible and Infrared Scanner (VIRS) aboard the TRMM



1 (Tropical Rainfall Monitoring Mission) satellite merged with other satellite-based
2 precipitation data and the Global Precipitation Climatology Centre (GPCC) rain gauge
3 analysis (Huffman et al., 2007).

4

5 **3 Methodology**

6 **3.1 Compiling a MODIS 0.1° x 0.1° gridded dataset**

7 To investigate the spatial and temporal variability of aerosols over the Eastern Mediterranean
8 we first created a 0.1° x 0.1° daily gridded aerosol dataset using single pixel level-2 AOD₅₅₀ and
9 FMR₅₅₀ data from MODIS Collection 051. The same resolution has been utilized in previous
10 studies (e.g. Barnaba and Gobbi, 2004) in the region; however, without reporting on the
11 gridding methodology followed. In this work we present a gridding methodology that could be
12 used as a reference for future regional studies. The methodology has been successfully applied
13 in the past on level-2 MODIS Terra data in different cases studies, e.g. in order to examine the
14 weekly cycle patterns of AOD₅₅₀ over the region of Central Europe and the aerosol load
15 changes observed over a cement plant in Greece due to changes in the deposition practices of
16 the primary materials (see Georgoulas and Kourtidis, 2012; Georgoulas et al., 2012; Kourtidis
17 et al., 2014). In the following lines we proceed to a detailed description of the method
18 underlining the potential of being used in detailed quantitative studies like this one.

19 First, a 0.1° x 0.1° resolution grid covering the Eastern Mediterranean (30°N-45°N, 17.5°E-
20 37.5°E) is defined which corresponds to 30000 grid cells. As already mentioned in Sect. 2.1,
21 only level-2 single pixel AOD₅₅₀ measurements with a QAC flag of 3 and a QAC flag greater
22 than 0 were used over land and over ocean, respectively, to ensure the high quality of the data.
23 Pixels are attributed at a specific grid cell if their center falls within a 25 x 25 km² square
24 window around the grid cell (see Fig. S1 in the Supplement). These pixels are then used for the
25 calculation of daily averages. As shown in Figure S1, a grid cell of 0.1° (~ 10 km) is as big as
26 the centre of a large Mediterranean city like Thessaloniki, Northern Greece (~ 1 million
27 inhabitants). The procedure was followed separately for MODIS Terra and Aqua data. In cases
28 of grid cells with no DT MODIS observations, data from the DB algorithm were used (over
29 bright arid and semi-arid regions of North Africa) constituting only a small part of the gridded
30 dataset.

31 The size of the gridding window was selected following Koukouli et al. (2007). They used both
32 10 and 25-km windows showing that the latter allows for the inclusion of more data points
33 without undermining the ability of monitoring accurately the aerosol load over a specific spot.



1 In addition, in cases of urban sites, a window of 25 km allows for the inclusion of pixels from
2 the surrounding non-urban surfaces where the MODIS surface reflectance parameterization is
3 better (Levy et al., 2010). The size of each MODIS pixel is 10 km at nadir, but at the swath
4 edges, it may become 2-3 times larger. Hence, ideally the maximum number of pixels that could
5 be used in the daily averaging is nine. The overlap between the windows of neighbouring grid
6 cells does not affect the representativeness of the dataset over each grid cell. Aerosols are
7 transported by air masses throughout the day and thus the aerosol load in neighbouring grid
8 cells is not expected to be completely independent.

9 In order to make sure that the use of a 25-km gridding window is optimal for capturing local
10 pollution sources we repeated the same procedure for bigger gridding windows (50-km, 75km
11 and 100-km) using MODIS Terra AOD₅₅₀ data for the year 2004. Numerous aerosol hot spots
12 cannot be seen as the gridding window becomes bigger and there is a significant smoothing of
13 the aerosol patterns mainly over land (Fig. S2). The use of the MODIS gridded dataset in the
14 detection of local aerosol hot spots is discussed in more detail in Sect. 4. In addition, we
15 conducted a detailed validation of the MODIS data against sunphotometric data from a total of
16 13 AERONET stations in the region (see Fig. 1). The validation procedure was repeated several
17 times for different spatial collocation windows which were equal to the windows used for the
18 gridding procedure (i.e. 25, 50, 75 and 100-km) and for different data quality criteria. The
19 results of the validation procedure are presented in Sect. 4.1 while part of them is given in the
20 Supplement of this manuscript (see Table S2). Overall, it is shown that the gridding
21 methodology followed here offers the best compromise for studying the spatial variability of
22 aerosols on a regional or local scale, preserving at the same time the representativeness of the
23 real aerosol load over each specific spot.

24 In order to generalize our results, nine different sub-regions (Fig. 1) were selected apart from
25 the three basic regions of interest, namely, the whole Eastern Mediterranean (EMT) and the land
26 (EML) and oceanic (EMO) areas of the region. The selection was done mainly taking into
27 account geographical but also land type and land use criteria. The four sub-regions that
28 correspond to the land regions of Eastern Mediterranean are the Northern Balkans Land (NBL),
29 the Southern Balkans Land (SBL), the Anatolia Land (ANL) and the Northern Africa Land
30 (NAL) region while the five sub-regions that correspond to the oceanic regions are the Black
31 Sea Oceanic (BSO), the North-Western Oceanic (NWO), the South-Western Oceanic (SWO),
32 the North-Eastern Oceanic (NEO) and the South-Eastern Oceanic (SEO) region. Mean values of



1 the total AOD₅₅₀ from the Terra and Aqua MODIS are reported for each one of the three basic
2 regions of interest and their nine sub-regions in Sect. 4.

3

4 **3.2 Contribution of different aerosol types to AOD₅₅₀**

5 **3.2.1 Ocean**

6 In order to quantify the contribution of different types of aerosols to the total AOD₅₅₀ we
7 followed a different approach for ocean and land regions. This is due to the lack of reliable
8 FMR₅₅₀ retrievals over land (e.g. see Levy et al., 2010; Georgoulias and Kourtidis, 2011) which
9 are crucial for the algorithms used in this work. Over ocean we utilize wind speed data at 10 m
10 above surface from the ERA-Interim reanalysis, AI data from TOMS and OMI along with
11 AOD₅₅₀ and FMR₅₅₀ from the MODIS Terra and Aqua gridded datasets presented above. All the
12 datasets were brought to the same 0.1 degree spatial resolution as MODIS by using bilinear
13 interpolation. In the case of TOMS and OMI we used monthly mean AI data following Bellouin
14 et al. (2008) in order to avoid gaps especially during the TOMS period.

15 In general, the algorithm used over oceanic regions (see Fig. 2) is similar with the one presented
16 in Bellouin et al. (2008). First, the marine AOD₅₅₀ (τ_m) is calculated from near surface wind
17 speed using a linear relation which has been obtained from ground-based studies over pollution
18 free oceanic regions. Bellouin et al. (2008) use the linear relation of Smirnov (2003). Then, if τ_m
19 is greater or equal than AOD₅₅₀ it is assumed that there are marine particles only over this
20 region. If τ_m is smaller than AOD₅₅₀ a decision tree is followed which is first based on FMR₅₅₀
21 and then on AI in order to reach a conclusion about the type of aerosols that account for
22 AOD₅₅₀. If FMR₅₅₀ is smaller than the critical value of 0.35 and AI is greater than or equal to a
23 critical value it is assumed that there are both marine aerosols (τ_m) and dust ($\tau_d = \text{AOD}_{550} - \tau_m$)
24 while if AI is smaller than this critical value it is assumed that there are marine aerosols only.
25 The AI critical value is equal to 1 in Bellouin et al. (2008). If FMR₅₅₀ is greater than or equal to
26 0.83 it is assumed that there are both anthropogenic ($\tau_a = \text{AOD}_{550} - \tau_m$) and marine aerosols (τ_m).
27 In the occasion of having a FMR₅₅₀ equal to 0.35 or greater than 0.35 but smaller than 0.83 one
28 has to take again AI into consideration. If AI is less than the critical value it is assumed that
29 there are marine aerosols (τ_m) only while in the opposite occasion it is assumed that all the three
30 types of aerosols that can be defined over oceanic regions by this algorithm, namely, dust
31 [$\tau_d = (1 - \text{FMR}_{550})(\text{AOD}_{550} - \tau_m)$], anthropogenic [$\tau_a = \text{FMR}_{550}(\text{AOD}_{550} - \tau_m)$] and marine aerosols (τ_m)
32 are present. One should keep in mind that all the biomass burning aerosols are classified as
33 anthropogenic by this method.



1 In this work, we proceeded to a "fine-tuning" of the algorithm for the region of Eastern
2 Mediterranean. First, we applied the algorithm on MODIS Terra data using the same critical
3 values as in Bellouin et al. (2008). The results showed that the original Bellouin et al. (2008)
4 method might be valid for global studies but for a "closed" sea like the Mediterranean the use of
5 the original critical values leads to a large overestimation of sea salt AODs and therefore
6 underestimation of dust and anthropogenic aerosol AODs. Indicative of this situation is Fig. S3
7 in the Supplement where we present the relative contribution of dust, marine and anthropogenic
8 aerosols per month over the oceanic regions of Eastern Mediterranean as calculated using the
9 original Bellouin et al. (2008) method. It is shown that the marine contribution is several times
10 higher than the values reported for the Mediterranean Basin in previous studies (e.g. see Nabat
11 et al., 2012). Evaluation of the algorithm was done using dust AOD₅₃₂ data from the LIVAS
12 CALIOP/CALIPSO product. From LIVAS we only use the high quality Sahara dust product as
13 a reference and not other aerosol type retrievals (e.g. marine aerosols) since the dust retrievals
14 from CALIOP/CALIPSO are by far the most reliable (e.g. Burton et al., 2013). We performed
15 several tests by changing the linear relation that connects τ_m with near surface wind speed and
16 the AI critical values and compared each time the dust AOD₅₅₀ seasonal variability with the
17 LIVAS AOD₅₃₂ seasonal variability for the ocean covered sub-regions of Eastern
18 Mediterranean. Results from this algorithm-tuning procedure can be found in Figs. S4e-i of the
19 Supplement where one can also see the underestimation of dust AOD₅₅₀ from the original
20 Bellouin et al. (2008) algorithm.

21 The linear relation given in Kaufman et al. (2005) was finally selected ($\tau_m=0.007ws+0.02$). The
22 2000-2012 average wind speed over the ocean for the region of Eastern Mediterranean is ~ 5.3
23 m/s. Kaufman et al. (2005) reduced the offset in the linear relation of Smirnov (2003) from 0.06
24 to 0.02 to fit the average baseline AOD of 0.06 for the typical wind speed of 6 m/s. In addition,
25 our tests showed that a AI critical value of 0.5 performs better over the region of Eastern
26 Mediterranean. As discussed in Jones and Christopher (2011), the AI threshold of 0.5 is capable
27 of separating sea salt from UV absorbing aerosols (dust and biomass burning) efficiently.
28 Another test, following the example of other studies (see Lehahn et al., 2010), was to assume
29 that for wind speed less than 5 m/s there is very little or no sea-spray particle production
30 (limited bursting of entrained air bubbles associated with whitecap formation). In this case, τ_m is
31 stable, equal to the offset of the linear relation between τ_m and wind speed which is indicative of
32 the background sea salt AOD₅₅₀. However, this test reveals that the effect of assuming stable τ_m
33 for wind speed less than 5 m/s is insignificant and therefore we selected to follow the Kaufman



1 et al. (2005) linear relationship for the whole wind speed range. As shown in Figs. S4e-i, the
2 seasonal variability when applying our modified algorithm over oceanic regions is very close to
3 the LIVAS dust AOD₅₃₂ especially for the months with lower dust load (June-January). It is also
4 shown that dust AODs from this algorithm are closer to the LIVAS dust product than dust
5 AODs from MACC reanalysis do. The slight overestimation of dust AOD or the shift of the
6 maximum dust load we observe for the period of high dust loads in the region (February-May)
7 is probably connected to the narrow swath and the 16-day time of CALIPSO which means that
8 several dust events might be not observed by the CALIOP instrument contrary to MODIS which
9 has a daily coverage.

10

11 **3.2.2 Land**

12 As already mentioned in the previous paragraph a different approach is followed over the land
13 regions of Eastern Mediterranean due the low confidence on the MODIS FMR₅₅₀ and Ångström
14 exponent retrievals over land compared to that over ocean (e.g. see Levy et al., 2010;
15 Georgoulas and Kourtidis, 2011). This limitation does not allow us to distinguish the
16 contribution of fine and coarse mode aerosols in terms of AOD₅₅₀. In this case, we choose to use
17 daily model fields of the dust contribution to the total AOD (here MACC reanalysis and
18 GOCART). We follow a method similar with the one presented in Bellouin et al. (2013).
19 Specifically, we calculate the dust AOD₅₅₀ by scaling the MODIS AOD₅₅₀ data with the MACC
20 or GOCART dust/total AOD₅₅₀ ratios [$f_d = \tau_{d(\text{model})} / \tau_{(\text{model})}$] on a daily basis.

21 Since the MACC data are available only from 2003 to 2012, in order to take advantage of the
22 full MODIS dataset (3/2000-12/2012), data from the GOCART model were used for the period
23 2000-2002. The GOCART data were normalized in order to be consistent with the MACC data.
24 Daily dust/total AOD₅₅₀ ratios (f_d) from the common GOCART-MACC period 2003-2007 were
25 first brought to a common 1° x 1° spatial resolution using bilinear interpolation and then we
26 calculated the regression line for each grid cell on a seasonal basis. The linear relations were
27 afterwards used in order to normalize the 2000-2002 GOCART ratios to have a homogeneous
28 dataset. The slopes and offsets of these regression lines and the corresponding correlation
29 coefficients (R) can be seen in Figs. S5, S6 and S7 of the Supplement, respectively. Overall, for
30 the whole time period, the MACC reanalysis f_d ratios are lower by ~ 26 % from the GOCART f_d
31 ratios and the linear relation connecting the two products is $f_{d\text{MACC}} = 0.4964f_{d\text{GOCART}} + 0.0952$
32 with a correlation coefficient R of 0.74. The f_d values of the merged GOCART-MACC (2000-
33 2012) timeseries were checked using the Standard Normalized Homogeneity Test (SNHT) as



1 described in Alexandersson (1986). The statistical significance was checked following Khaliq
2 and Ouarda (2007) and the f_d timeseries were found to be homogeneous (see Fig. S8 of the
3 Supplement). Hence, this test verifies that the use of the merged GOCART-MACC f_d dataset
4 will not insert any artifacts (e.g. trends or breaks) in the algorithm. Finally, the f_d data were
5 brought to the same spatial resolution with MODIS data ($0.1^\circ \times 0.1^\circ$) using bilinear interpolation
6 again.

7 After the calculation of τ_d with the use of f_d values ($\tau_d = f_d AOD_{550}$), we proceed to the calculation
8 of the anthropogenic contribution to the total AOD_{550} (τ_a) by multiplying the non-dust part of
9 AOD_{550} with the anthropogenic fraction f_a for the region of Eurasia (0.77 ± 0.20) given in
10 Bellouin et al. (2013) [$\tau_a = f_a(1 - f_d)AOD_{550}$]. The rest of the total AOD_{550} is attributed to the fine
11 mode natural aerosols [$\tau_n = (1 - f_a)(1 - f_d)AOD_{550}$] (see Fig. 2). As discussed in Bellouin et al.
12 (2013), the fine mode natural aerosols consist of sea salt, dimethyl sulfide from land and
13 oceanic sources, SO_2 from degassing volcanoes and secondary organic aerosols from biogenic
14 emissions. It has to be highlighted that like in the case of oceanic regions the biomass burning
15 aerosols are classified as anthropogenic by this algorithm. As shown in Figs. S4a-d, the seasonal
16 variability of τ_d over land covered regions is very close to the LIVAS dust AOD_{532} which is
17 used as a reference.

18 Overall, the algorithm described above performs well as far as dust is concerned. This is further
19 shown when comparing MODIS Terra and Aqua τ_d values with collocated AERONET
20 observations for dust dominated days (see Fig. S9 in the Supplement). The method followed for
21 the collocation of the data is similar to the one presented in Sect. 4.1 while dust dominated days
22 were days with an AERONET AE smaller than 1 (see Mateos et al., 2014) and a MODIS based
23 τ_d greater than τ_a and τ_n or τ_m . The uncertainties of the calculated τ_a , τ_d , τ_n and τ_m values which
24 are inserted by the input data and the assumptions of the algorithm are expected to be similar
25 with the ones presented in Bellouin et al. (2013). Bellouin et al. (2013) using a Monte-Carlo
26 analysis indicated that τ_a can be specified with an uncertainty of $\sim 23\%$ over land and $\sim 16\%$
27 over the ocean, τ_d can be specified with an uncertainty of $\sim 19\%$ over land and $\sim 33\%$ over the
28 ocean, τ_n can be specified with an uncertainty of $\sim 41\%$ and τ_m with an uncertainty of $\sim 28\%$.
29 The results of the application of the algorithm described in the paragraphs above are presented
30 in the following section (Sect. 4) by means of maps, pie charts, plots and tables for each one of
31 the three basic regions of interest and their nine sub-regions.

32



1 **4 Results and discussion**

2 **4.1 Validation of MODIS gridded data using ground-based observations**

3 As discussed in Sects. 2 and 3, the high quality (QAC: 3) DT level-2 Collection 051 MODIS
4 data used in this work were validated in detail against data from 13 AERONET stations (see
5 Fig. 1). The stations were selected to make sure that their version 2.0 level 2.0 high quality
6 cloud screened Cimel sunphotometric observations were covering at least 2 years and there
7 were at least 100 common days of AERONET and MODIS observations. The exact
8 geolocation of the AERONET stations is given in Table 1 (see also Fig.1) along with the
9 period of available data, the hosting country, the type of the station (e.g. urban/rural,
10 coastal/continental, etc.) and the corresponding mean overpass time of Terra and Aqua
11 MODIS. First, we collocated spatially and temporally the MODIS and AERONET
12 observations by temporally averaging AERONET measurements within ± 30 min from the
13 MODIS overpass time (see Levy et al., 2010) and spatially averaging MODIS measurements
14 centered within a 25×25 km² window around each station (see Koukouli et al., 2010). The
15 use of a collocation window equal to the one used for the gridding procedure, practically,
16 allows us to validate at the same time the $0.1^\circ \times 0.1^\circ$ MODIS gridded product.

17 The regression lines between MODIS and AERONET AODs are shown in Fig. 3 while
18 details about the validation results can be found in Table 2. Overall, the MODIS Terra DT
19 Collection 051 data overestimate AOD₅₅₀ by 11.59 % (Normalized Mean Bias - NMB) with
20 63.28 % of the data falling within the expected error (EE) envelope and 67.78% within the
21 pre-launch expected error (pLEE) envelope. The expected error envelope is define as: $AOD -$
22 $|EE| \leq AOD_{MODIS} \leq AOD + |EE|$ with EE being $\pm(0.05 \pm 0.15AOD)$ (Levy et al., 2010) and
23 pLEE being $\pm(0.05 \pm 0.20AOD)$ (Kaufman et al., 1997). On the other hand, the MODIS Aqua
24 DT Collection 051 data overestimate AOD₅₅₀ by 25.18 % (NMB) with 57.14 % of the data
25 falling within the EE envelope and 61.87 % within the pLEE envelope. The percentage of the
26 MODIS Terra and Aqua data falling within the EE envelope are close to the 57 % given in
27 Remer et al. (2005) for Eastern Mediterranean. The validation results for each station
28 separately can be found in Table S1 of the Supplement. The results discussed in this
29 paragraph are comparable to the ones appearing in previous studies focusing on the
30 Mediterranean region (see Papadimas et al., 2009; Koukouli et al., 2010). In general, it is
31 shown here that the MODIS Terra Collection 051 data exhibit a better agreement with the
32 ground-based observations from AERONET than MODIS Aqua data do.



1 To be in line with the global validation of the DT Collection 051 product by Levy et al.
2 (2010) we also performed a validation with the specifications used in their work. We used a
3 50 x 50 km² window for the spatial collocation of the MODIS and AERONET data while
4 only days with at least 5 MODIS retrievals and 2 AERONET measurements were taken into
5 account. The increased size of the collocation window improves the results of the validation.
6 As shown in Table 2, MODIS Terra DT Collection 051 data overestimate AOD₅₅₀ by 5.10 %
7 (NMB) with 70.17 % of the data falling within the EE envelope and 74.64 % within the pLEE
8 envelope. For MODIS Aqua, the NMB is 15.34%, while the percentage of the measurements
9 falling within the EE and pLEE envelope is 66.76 % and 70.45 %, respectively. These results
10 about Eastern Mediterranean are close to the global ones presented in Levy et al. (2010).
11 As discussed in Sect. 3.1, data from the DB algorithm were used over bright arid and semi-
12 arid regions of North Africa for the production of the 0.1° x 0.1° MODIS gridded dataset for
13 grid cells with no DT data. Therefore, in this work we also perform a validation of the DB
14 Collection 051 product over the region of Eastern Mediterranean. In the case of DB data, we
15 first make use of all the available DB observations without any quality filtering over the 13
16 AERONET stations. A spatial window of 25-30 km has been typically used in the past for the
17 collocation of MODIS DB data with the AERONET observations (see Shi et al., 2011;
18 Ginoux et al.; 2012; Sayer et al., 2013; 2014) which is in line with the 0.25 x 0.25 km²
19 window used here. The MODIS Terra DB data overestimate AOD₅₅₀ by 21.38 % (NMB) with
20 51.90 % of the data falling within the expected uncertainty envelope assuming a DB expected
21 uncertainty of $\pm 0.05 \pm 20\%AOD_{AERONET}$ (Hsu et al., 2006). The MODIS Aqua DB Collection
22 051 data overestimate AOD₅₅₀ by 33.03 % (NMB) with 55.30 % of the data falling within the
23 expected uncertainty envelope. We repeated the validation procedure for DB data taking into
24 account the highest quality data only. The sample of available measurements was diminished
25 by a factor of 5 in the case of MODIS Terra and 6 in the case of MODIS Aqua but the results
26 were pretty similar with the ones for the unfiltered data. Therefore, the use of unfiltered DB
27 data during the gridding procedure does not insert any significant uncertainty. The DB results
28 for the 13 AERONET stations examined here are not of the same agreement than the DT
29 results and the ones presented in previous studies utilizing DB Collection 051 data for other
30 stations and larger regions (see Shi et al., 2011; Ginoux et al., 2012). However, it has been
31 reported that stations in the region (e.g. Sede Boqer in Israel) are among the ones with the
32 greatest discrepancies between MODIS DB and AERONET measurements (Ginoux et al.,
33 2012). Nevertheless, as commented in Sect. 3.1, the DB data constitute only a small fraction



1 of the data used for the production of the MODIS gridded dataset (~ 1 % only of the 30000
2 grid cells covering Eastern Mediterranean has only DB retrievals) and therefore they do not
3 affect significantly its quality.

4 As discussed in Sect. 3.1 the gridding procedure was repeated four times using a gridding
5 window of 25, 50, 75 and 100-km using MODIS Terra AOD₅₅₀ data for the year 2004 showing
6 that the 25-km window is optimal for capturing local pollution sources. In order to see how the
7 size of the gridding window affects the agreement between MODIS and AERONET data we
8 also proceeded to a validation of MODIS DT data against AERONET measurements using
9 different spatial collocation windows (25, 50, 75 and 100-km) and two quality criteria, a "strict"
10 one: at least 2 AERONET measurements for each MODIS-AERONET pair and "stricter" one:
11 at least 5 MODIS retrievals and 2 AERONET measurements for each MODIS-AERONET pair
12 as in Levy et al. (2010). The results for the DT MODIS Terra and Aqua data are presented in
13 Table S2 of the Supplement. In general, it is shown that the increased size of the spatial
14 collocation window leads to an improvement of the bias between satellite and ground-based
15 observations. This is probably due to the inclusion of more observations into the calculations
16 which diminishes the noise of the MODIS observations. In addition, as expected, the stricter
17 quality criteria lead to a better agreement between MODIS DT and AERONET data. Taking
18 into account not only the NMB but also the regression lines and the other metrics appearing in
19 Table 2S, it is concluded that the 50-km window is the best choice for the validation procedure
20 in line with Ichoku et al. (2002). On the other hand, the 25-km validation results are close to the
21 50-km ones (see Table S2) and at the same time the 25-km gridding window allows for a more
22 efficient detection of local aerosol sources as shown in Sect. 3.1. Taking into account this, we
23 suggest that the 25-km window used for the production of the 0.1° x 0.1° gridded MODIS
24 dataset is the optimal selection for studying the spatial variability of aerosols, preserving at the
25 same time the representativeness of the real aerosol load over each specific spot.

26

27 **4.2 Aerosol spatial variability and hot spots**

28 The AOD₅₅₀ spatial variability over the greater Eastern Mediterranean region for the period
29 2000-2012 as seen from the Terra MODIS 0.1° x 0.1° dataset is presented in Fig. 4. Several
30 aerosol hot spots that coincide with megacities (e.g. Cairo, Istanbul), large cities (e.g. Athens,
31 Ankara, Alexandria, Izmir, Thessaloniki) or even medium sized cities (e.g. Larissa,
32 Limassol), industrial zones (e.g. OSTIM Industrial Zone in Ankara, Turkey), power plant
33 complexes (e.g. Maritsa Iztok complex at the Stara Zagora Province in Bulgaria, Ptolemaida-



1 Kozani power plants in Western Macedonia, Greece), river basins (e.g. Evros river Basin at
2 the borders between Greece and Turkey), etc. can be detected on the map. Indicatively, in Fig
3 4 we give a list of 35 local particle pollution sources in the region; however, careful
4 inspection of this map and the seasonal maps presented in Fig. 6 allows for the detection of
5 many more aerosol sources. The results from the analysis of Aqua MODIS data are pretty
6 similar as shown in Fig. S10 of the Supplement. A significant number of the local aerosol
7 sources can also be detected on the OMI 2004-2012 tropospheric NO₂ and PBL SO₂ maps
8 given in Figs. 5a and b which reveals the origin of aerosols over these regions (e.g. traffic,
9 industrial activities, etc). However, there are regions of high aerosol load which cannot be
10 seen in Fig. 5a and b and vice versa which is indicative of the significant role of other
11 anthropogenic or natural processes that contribute to the local aerosol load (e.g. fires, soil dust
12 from agricultural activities or arid regions, Sahara dust transport).

13 The topography (Fig. 5c) and precipitation (see Fig. 5d for annual precipitation levels for the
14 period 2000-2012 from TRMM) are also major determinants of the local AOD₅₅₀ levels. For
15 example, regions with mountain ranges on the Balkan Peninsula (e.g. Pindus mountain range
16 in Greece, Dinaric Alps that run through Albania and the former Yugoslav republics, the
17 Balkan mountain range in Central Bulgaria) are characterized by low AODs (see Fig. 4). On
18 the contrary, regions of low altitude are generally characterized by higher AODs because the
19 majority of anthropogenic activities is usually concentrated there. Also, low altitude regions
20 surrounded by high mountains are characterized by higher AODs as aerosols cannot be easily
21 transported by the wind (e.g. the industrialized regions in Central Bulgaria which are confined
22 between the high Balkan and Rodopi mountain ranges). As precipitation is the major removal
23 mechanism of pollutants in the atmosphere, regions with high AOD₅₅₀ are in many cases
24 connected to low precipitation levels and vice versa (see Figs. 4 and 5d). A striking example
25 is the one of Anatolia in Central Turkey which is characterized by lower precipitation levels
26 and higher aerosol loads compared to the surrounding regions. Also, the low precipitation
27 levels are partly responsible for the high aerosol loads appearing over Northern Africa.

28 Overall, the mean AOD₅₅₀ for the whole period of interest is estimated at 0.215 ± 0.187 for
29 Terra and 0.217 ± 0.199 for Aqua MODIS for the Eastern Mediterranean region which is ~ 45
30 % higher than the global average appearing in recent studies (e.g. Kourtidis et al., 2015). Over
31 land higher mean AODs are generally recorded (0.219 ± 0.165 for Terra and 0.239 ± 0.189
32 for Aqua MODIS) than over the ocean (0.213 ± 0.201 for Terra and 0.202 ± 0.205 for Aqua



1 MODIS). All these values along with the mean AODs for the 9 sub-regions of interest
2 covering Eastern Mediterranean can be found in Table 3.

3 The AOD₅₅₀ spatial variability on a seasonal basis from MODIS Terra and Aqua is presented
4 in Fig. 6 along with the difference between the two products. The majority of the local aerosol
5 sources over land are more prominent in summer due to the limited washout by precipitation
6 (see also Papadimas et al., 2008) and also due to the enhanced photochemical production of
7 secondary organic aerosols (Kanakidou et al., 2011 and references therein). In addition,
8 during summer, over the region, there is typically a significant transport of aerosols (e.g. see
9 Kanakidou et al., 2011 and references therein) and gaseous pollutants like SO₂ and NO₂ (see
10 Georgoulas et al., 2009; Zyrichidou et al., 2009) and biomass burning aerosols from Central-
11 Eastern Europe. Over the ocean, a profound maximum is observed in spring which is due to
12 the well documented transport of significant amounts of dust from the Sahara Desert
13 extending across the North African coast and the ocean. The seasonal variability of aerosols
14 and the relative role of different aerosol types and various processes is discussed in more
15 details in Sect 4.4.

16 The difference between MODIS Terra and Aqua Collection 051 AOD₅₅₀ over Eastern
17 Mediterranean is -0.002 (-1.40 %) for winter, -0.009 (-3.27 %) for spring, -0.011 (-4.46 %) for
18 summer and 0.008 (4.40 %) for autumn. AOD₅₅₀ levels from Terra MODIS are lower than
19 that from Aqua MODIS over land for all seasons. Over the sea, Terra MODIS AOD₅₅₀ levels
20 are lower than that of Aqua MODIS only in winter. The fact that Terra MODIS measurements
21 are systematically higher than that from Aqua over the ocean by ~ 0.01 on an annual basis is
22 in line with the findings of previous global studies for Collection 5 (e.g. Remer et al., 2006;
23 2008). Locally, one can see regions with positive and negative differences between Terra and
24 Aqua MODIS AOD₅₅₀. The patterns of the Terra-Aqua difference per season are presented in
25 Figs. 6c, f, i and l while the patterns of the percent difference are given in Fig. S11 of the
26 Supplement. The largest part of the Terra-Aqua MODIS differences over land and ocean
27 observed here may be attributed to the known calibration and sensor degradation issues of
28 MODIS (for details see Levy et al., 2010; 2013; Lyapustin et al., 2014). A significant effort
29 has been undertaken to address these issues in the new (Collection 6) MODIS product (e.g.
30 Levy et al., 2013; Lyapustin et al., 2014) and a repetition of a similar analysis with Collection
31 6 data in the future would be a valuable contribution. Taking into account the aforementioned
32 issues and the retrieval uncertainty of MODIS it becomes more than obvious that the
33 attribution of observed differences between Terra and Aqua to the diurnal variability of



1 aerosol load (e.g. over biomass burning regions) in the region is a difficult task. It is shown in
2 Fig. S12 of the Supplement that the diurnal variability of AOD₅₅₀ from AERONET ranges
3 significantly from station to station. The average hourly departure from the daily mean for the
4 total of the 13 stations ranges from ~ -5 % to ~ 5 %. Specifically, for the MODIS Terra and
5 Aqua overpass times, the AERONET AOD₅₅₀ difference ranges from ~ -10 % to ~ 10 % (see
6 Fig. S12b). The Terra-Aqua AOD₅₅₀ difference is negative for the total of the 13 stations
7 ranging from ~ -25 % to ~ -5 %. It is shown in Fig. S12b that the two differences exhibit a
8 similar variability from station to station which indicates that part of the observed Terra-Aqua
9 difference is indeed due to the diurnal variability of aerosols. However, as mentioned above,
10 the diurnal variability of aerosols is a very delicate issue and should be comprehensively
11 addressed in a future study. The same stands for other kind of variabilities which could be
12 connected to local and regional anthropogenic activities like e.g. the weekly cycle of aerosols
13 (see Georgoulias and Kourtidis, 2011; Georgoulias et al., 2015).

14

15 **4.3 Contribution of different aerosol types to the total AOD₅₅₀**

16 **4.3.1 Annual contribution**

17 As mentioned above, we attempt to estimate in our work the contribution of different aerosol
18 types to the total AOD₅₅₀ over the region of Eastern Mediterranean was calculated following
19 the methodology presented in Sect. 3.2. For the land covered areas, based on MODIS Terra
20 observations, we estimate that 52 % (0.112±0.087) of the total AOD₅₅₀ is due to
21 anthropogenic aerosols, 32 % (0.074±0.080) due to dust and 16 % (0.034±0.026) due to fine
22 mode natural aerosols (see Fig. 7). For the oceanic areas, 41 % (0.086±0.085) of the total
23 AOD₅₅₀ is due to anthropogenic aerosols, 34 % (0.076±0.185) due to dust and 25 %
24 (0.054±0.018) due to marine aerosols (see Fig. 7). The results based on observations from
25 MODIS Aqua are similar. Over land, 50 % (0.117±0.093) of the total AOD₅₅₀ is
26 anthropogenic, 35 % (0.090±0.102) is due to dust and 15 % (0.035±0.028) due to fine mode
27 natural aerosols, while, over ocean, 40 % (0.079±0.080) of the total AOD₅₅₀ is of
28 anthropogenic origin, 33 % (0.070±0.181) is due to dust and 27 % (0.054±0.018) due to
29 marine aerosols (see Fig. 7). These results along with the relative contributions and the annual
30 τ_a , τ_d , τ_n and τ_m levels for each one of the nine sub-regions of interest (see Fig. 1) are given in
31 Table 4.

32 For anthropogenic aerosols, the region with the highest relative contribution is NBL (59 % for
33 both Terra and Aqua MODIS) while the region with the lowest relative contribution is SWO



1 (32 % for both Terra and Aqua MODIS) (see also Table 4). The spatial variability of τ_a is
2 presented in Fig. 8a for Terra MODIS and Fig. S13a of the Supplement for Aqua MODIS, the
3 patterns being similar in both cases. Over land, the annual τ_a patterns are similar to the
4 AOD₅₅₀ patterns, the highest values appearing over local particle pollution sources (cities,
5 industrial zones, etc.). Over the sea, τ_a is higher along the coasts, while it drops significantly
6 towards other directions. An interesting feature here is that the oceanic region of Black Sea
7 (BSO) presents higher relative anthropogenic contributions than the rest of the oceanic sub-
8 regions but also than land areas with significant anthropogenic sources (e.g. ANL and NAL).
9 This is indicative of the transport of atmospheric particles from Central Europe and biomass
10 burning aerosols during the biomass burning seasons in April-May from Russia (across the
11 latitudinal zone 45°N-55°N) and July-August from South-Western Russia and Eastern Europe
12 (Amiridis et al., 2010). These aerosols are transported at much lower latitudes as shown in
13 previous studies (e.g. Vrekoussis et al., 2005; Karnieli et al., 2009) reaching the Sahara Desert
14 and the Middle East regions (Pozzer et al., 2015). The fact that τ_a drops gradually from the
15 coasts is also seen in Fig. 9 where the latitudinal variability of the optical depths of the
16 different aerosol types (τ_a , τ_d , τ_n and τ_m) is presented for four bands that cover the whole
17 Eastern Mediterranean. An interesting feature is that τ_a increases nearby the shoreline
18 (particularly along the North African coastal zone) before it gradually decreases. Over land
19 aerosols are located within the atmospheric boundary layer, close to the emission sources, and
20 hence, their deposition and removal from the atmosphere is more efficient than over the
21 ocean. The particles which are transported over the ocean on the other hand usually reach
22 greater heights which prolongs their lifetime.

23 As shown in Fig. 9, the same feature is observed for dust. Indicatively, τ_d and the relative
24 contribution of dust to the total AOD₅₅₀ on an annual basis over the oceanic regions of SWO
25 and SEO are in general higher or comparable to the ones over NAL (see Table 4 for more
26 details). In Fig. 9, the MODIS-based τ_d latitudinal variability is presented along with the
27 latitudinal variability of dust AOD₅₃₂ and extinction coefficients of dust at 532 nm from
28 LIVAS. As expected, in all cases τ_d decreases with distance from the large dust sources in the
29 South and South-East (Sahara Desert, Middle East deserts) with local maxima over the
30 latitudinal zone from 35°N to 40°N (especially for band 2 and band 3). The latitudinal
31 variability of τ_d is similar to the latitudinal variability of dust AOD₅₃₂ for all the four bands
32 despite the fact that the MODIS-based data have a resolution 100 times higher (0.1° vs 1°) and
33 therefore are more sensitive to local characteristics. Dust reaches heights up to ~ 4-5 km in the



1 area; however, the largest fraction of dust mass is confined within the first 2-3 km of the
2 troposphere (see Fig. 9). The annual τ_d patterns are shown in Fig. 8b for Terra MODIS (Fig.
3 S13b of the Supplement for Aqua MODIS). The main dust transport pathways over the
4 oceanic areas of Eastern Mediterranean can be seen along with various local maxima over
5 land. The highest τ_d values over land appear over the regions of NAL and ANL (see Table 4)
6 and along the coasts. The high dust concentrations appearing over these regions are not only
7 due to the transport of dust from the nearby deserts but also due to local dust sources. A
8 recent study by Liora et al. (2015) reports various local sources of wind blown dust along the
9 coastal regions of Greece and Turkey, over the region of Anatolia in Turkey, over the Greek
10 islands, Crete, Cyprus and regions close to the coastal zone of Middle East. Their results are
11 in good agreement with the τ_d patterns presented in this work.

12 As shown in Fig. 7, fine mode natural aerosols exhibit the lowest contribution to the total
13 AOD₅₅₀ compared to the other aerosol types over land. The spatial variability of τ_n is very low
14 compared to τ_a and τ_d as shown in Figs. 8c and 9. It is inferred from the values appearing in
15 Table 4 that τ_n increases slightly as one moves from North to South; however, the relative
16 contribution of fine mode natural aerosols to the total AOD₅₅₀ slightly decreases (i.e. 17.67 %
17 over NBL and 14.97 % over NAL according to Terra MODIS observations). The latitudinal
18 variability and the percentages appearing in Table 4 are in accordance to the relative
19 contributions of biogenic aerosols to the total AOD₅₅₀ appearing over Eastern Mediterranean
20 in a recent modeling study (Rea et., 2015).

21 Similar to fine mode natural aerosols over land, marine aerosols generally have the lowest
22 contribution to the total AOD₅₅₀ compared to the other aerosol types over the sea (see Fig. 7
23 and Table 4) except for BSO. The variability of τ_m is very low compared to τ_a and τ_d . On an
24 annual basis, high τ_m values appear over the Aegean Sea and the oceanic area between Crete
25 and the North African coast while slightly lower values appear along the coasts of Eastern
26 Mediterranean (see Figs. 8d and 9). The τ_m patterns follow the near surface wind speed
27 patterns in the region (see Fig. S14 of the Supplement) being in accordance to the τ_m , marine
28 particulate matter concentration or sea salt emission patterns appearing in other studies (Im et
29 al., 2012; Nabat et al., 2013; Rea et al., 2015; Liora et al., 2015).

30

31 **4.3.2 Seasonal contribution**

32 The contribution of different aerosol types to the total AOD₅₅₀ over the Eastern Mediterranean
33 varies from season to season. The relative contribution of each aerosol type over EML and



1 EMO for each season is shown in Fig. 10. Over land, the relative contribution of τ_a , τ_d and τ_n
2 to the total AOD_{550} exhibits a low seasonal variability. The relative contribution of
3 anthropogenic aerosols to the total AOD_{550} ranges from 49 % in SON to 50 % in DJF based
4 on Terra MODIS observations and from 48 % in MAM and SON to 52 % in JJA based on
5 Aqua MODIS observations. In contrast, over the oceanic regions the relative contribution of
6 τ_a , τ_d and τ_m to the total AOD_{550} exhibits a significant seasonal variability. The relative
7 contribution of anthropogenic aerosols to the total AOD_{550} ranges from 27 % / 27 % in DJF to
8 50 % / 47 % in JJA based on Terra/Aqua MODIS observations. The percentages appearing
9 here are in accordance to the values appearing in Hatzianastassiou et al. (2009) where a
10 different satellite-based approach was followed. Indicatively, for the greater Athens area, an
11 average summertime anthropogenic contribution of ~ 50 % was found here based on Terra
12 MODIS data which is within the summer period range of 47-61 % indicated in the study by
13 Hatzianastassiou et al. (2009). In addition, the corresponding values for the greater
14 Thessaloniki area, Crete, Cairo and Alexandria are 53 %, 38 %, 48 % and 41 %, respectively,
15 within the range of values (57-73 %, 36-52 %, 34-56 % and 23-60 %) shown in
16 Hatzianastassiou et al. (2009). Only in the case of Ankara, our results suggest a lower
17 anthropogenic contribution (52 % versus 71-84 %). Particularly for Athens, Gerasopoulos et
18 al. (2011) following a different approach incorporating ground-based AOD observations and
19 trajectory modeling reached similar results (annual contribution of ~ 62 % from local and
20 regional sources and continental Europe which is expected to be mostly of anthropogenic
21 origin). Similarly, for Crete, Bergamo et al. (2008) using a different approach, also utilizing
22 ground-based data, found an annual anthropogenic contribution of ~ 43 %.

23 The seasonal patterns of the anthropogenic aerosols (τ_a) over the Eastern Mediterranean based
24 on MODIS Terra observations are presented in Figs. 11a, e, i and m while the seasonal
25 variability of τ_a over the whole region, over the land covered part and the oceanic part and
26 over the 9 sub-regions of interest is presented in Fig. 12. The results based on MODIS Aqua
27 observations are similar and can be found in Figs. S15a, e, i and m and Fig. S16 of the
28 Supplement. Generally, the local hot spots are detectable throughout the year; however, they
29 are becoming much more discernible in spring and especially in summer. As shown in Fig.
30 12a, τ_a nearly doubles during the warm period of the year (spring-summer) with the seasonal
31 variability being stronger over the sea (Fig. 12c) than over land (Fig. 12b). A clear peak is
32 observed in summer, August being the month with highest τ_a levels. As discussed in Sect.
33 4.3.1 the summer peak is mostly a result of three basic reasons. The first one is the deficiency



1 of wet removal processes compared to the cold period. As shown in Fig. S17, based on the
2 TRMM satellite observations, August and July are the months with the lowest precipitation
3 levels over the land covered part (a drop of ~ 75 % compared to winter months) and over the
4 oceanic part (a drop of ~ 90 % compared to winter months) of Eastern Mediterranean,
5 respectively. The second reason is the enhancement of the photochemical production of
6 secondary organic aerosols in summer (Kanakidou et al., 2011) and the third reason is the
7 transport of pollution aerosols from Central Europe and biomass burning aerosols from South-
8 Western Russia and Eastern Europe during the biomass burning season in July-August
9 (Amiridis et al., 2010). The Etesians, which are persistent northerly winds that prevail over
10 Eastern Mediterranean during summer, bring dry and cool air masses and aerosols from the
11 regions mentioned above while blocking at the same time the transport of desert dust in the
12 region and dispersing local pollution in urban areas to levels typical for rural areas (see Tyrllis
13 and Lelieveld, 2013 and references therein). As seen in Figs. 12a-l, a smaller but distinct in
14 most cases τ_a peak appears in April mostly as a result of the transport of biomass burning
15 aerosols from Russia (across the latitudinal zone 45°N-55°N). This is in line with the findings
16 of Sciare et al. (2008) who detected traces of these biomass burning aerosols at the island of
17 Crete in Southern Greece.

18 As discussed above, the relative contribution of dust to the total AOD₅₅₀ over land exhibits a
19 low seasonal variability ranging from 29 % in DJF to 36 % in SON based on Terra MODIS
20 observations and from 33 % in JJA to 38 % in SON based on Aqua MODIS observations (see
21 Fig. 10). Over the oceanic regions the relative contribution of dust to the total AOD₅₅₀ ranges
22 significantly throughout a year from 26 % / 28 % in JJA to 42 % / 39 % in MAM based on
23 Terra/Aqua MODIS observations. The percentages appearing here are in accordance to model
24 and observational studies. For example, de Meij et al. (2012) using the atmospheric chemistry
25 general circulation model EMAC (ECHAM/MESSy Atmospheric Chemistry) showed that
26 dust contributes on an annual level ~ 30 % to the total AOD₅₅₀ over stations located in the
27 area of Eastern Mediterranean. Gerasopoulos et al. (2011) found a ~ 23 % percent
28 contribution of North African dust to the total AOD over Athens using ground-based AOD
29 observations and trajectory modeling. Taking into account that part of the ~ 39 % local and
30 regional sources appearing in Gerasopoulos et al. (2011) is due to local dust sources,
31 especially in summer, turns out that their results are in agreement with the ~ 33 % relative
32 contribution found in this work for the greater Athens area based on Terra MODIS
33 observations. The seasonal patterns of dust (τ_d) over the region based on Terra MODIS



1 observations are shown in Figs. 11b, f, j and n while the seasonal variability of τ_d over the
2 whole region, over land, over the sea and over the 9 sub-regions of interest is shown in Fig.
3 12. The corresponding results based on MODIS Aqua observations are pretty similar and can
4 be found in Figs. S15b, f, j and n and Fig. S16 of the Supplement.

5 As seen in Fig. 11f, in spring, mostly due to the strong Sahara dust events, very high τ_d values
6 appear over land regions in North Africa, Middle East, Anatolia and oceanic areas across
7 Eastern Mediterranean (especially below 35°N). Dust loading over the sea exhibits two
8 maxima, one at the coastal zone of Libya and one across the coastal zone of Middle East. The
9 same two maxima but with much lower τ_d values appear in summer (Fig. 11j) and autumn
10 (Fig. 11n). Over land, the τ_d patterns are similar in summer and autumn, the maximum values
11 appearing over the Anatolian Plateau and areas of North Africa and Middle East. During
12 winter, dust maxima appear across the coastal zone of Northern Africa with relatively low τ_d
13 values across the coastal zone of Middle East (Fig. 11b). In winter τ_d levels are low over land
14 compared to the other seasons (Figs. 11b, f, j and n) as precipitation levels (see Fig. S17 of the
15 Supplement) and hence wet scavenging of aerosols peak. At the same time, the local
16 emissions of dust are low for regions away from the large area sources in the South (Liora et
17 al., 2015). In contrast, over the sea τ_d levels in winter are similar or slightly higher for some
18 areas than that in summer and autumn (see Figs. 11 and 12) as this is the season with the
19 second highest frequency (after spring) of strong (~ 21 %) and extreme (~ 26 %) desert dust
20 episodes in the region (see Gkikas et al., 2013 for details). February is by far the winter month
21 the highest τ_d levels (see Fig. 12) in line with the findings of Pey et al. (2013) who showed
22 that the intensity of African dust episodes over stations in Greece and Cyprus peaks in
23 February. Dust exhibits a strong peak in spring, April being the month with the highest τ_d
24 levels in line with other studies (e.g. Israelevic et al., 2012; Varga et al., 2014). The peak in
25 April is a result of the high cyclonic activity over North Africa during this month as shown by
26 Flaounas et al. (2015). According to the same study, low pressure systems are responsible for
27 ~ 10-20 % of moderate and ~ 40-50 % of high and extreme Sahara dust transport events over
28 Eastern Mediterranean. North Africa (Sharav) cyclones develop mainly in spring and summer
29 while Mediterranean cyclones develop in winter and autumn. The Mediterranean cyclones are
30 more intense than Sharav cyclones. The region, is also affected by events bringing particles
31 from dust source regions in the eastern part of Mediterranean basin (Negev desert in Israel,
32 Sinai in Egypt, Anatolian Plateau in Turkey) and the Arabian deserts (Basart et al. 2009; Pey
33 et al., 2013; Abdelkader et al., 2015). Dust remains in the atmosphere for a period of 1-4 days



1 undergoing chemical aging before being removed (see Abdelkader et al. 2015 and references
2 therein). The seasonal variability of τ_d is much stronger and the spring maxima much more
3 prominent over the sea (see Fig. 12). This is expected, as dust is only occasionally transported
4 over the sea during episodic events, while over land, local sources also contribute to the dust
5 burden especially in summer due to the dryness of soil. For example, over NBL, a broad
6 spring-summer peak is observed, June being the month with the highest τ_d levels. As one
7 moves south (SBL, ANL and NAL) the April peak becomes more prominent.

8 The relative contribution of fine mode natural aerosols to the total AOD_{550} over land exhibits
9 a very low seasonal variability ranging from 15 % in MAM and SON to 16 % in DJF and JJA
10 based on Terra MODIS observations and from 14 % in DJF and SON to 15 % in MAM and
11 JJA based on Aqua MODIS observations (see Fig. 10). The seasonal variability is also very
12 low, the highest values appearing in spring and summer (Fig. 12). Despite the generally low
13 contribution of fine mode natural aerosols to the total AOD_{550} over Eastern Mediterranean, τ_n
14 levels are similar to τ_d levels during winter months over specific regions (NBL and SBL). The
15 low seasonal variability can also be seen in Figs. 11c, g, k and o where the patterns of fine
16 mode natural aerosols (τ_n) are presented.

17 The seasonal relative contribution of marine aerosols to the total AOD_{550} over the oceanic
18 regions of Eastern Mediterranean is shown in Fig. 10. τ_m ranges from 20 % in MAM to 35 %
19 in DJF based on Terra MODIS observations and from 21 % in MAM to 36 % in DJF based on
20 Aqua MODIS observations (see Fig. 10). Like in the case of fine mode natural aerosols, the
21 seasonal variability is very low, but here the highest values appear in winter (Fig. 12). Due to
22 the linear relation of τ_m and near surface wind speed within our algorithm (see Fig. 2) the τ_m
23 seasonal variability and patterns follow the wind speed ones (see Figs. 11d, h, l, p and S14).
24 Marine aerosol concentrations are lower close to the coastlines while the highest
25 concentrations (see Liora et al., 2015) and τ_m values within Eastern Mediterranean appear
26 over the Aegean Sea (see Fig. 11). Overall, the τ_m patterns are in accordance to the τ_m , marine
27 particulate matter concentration and sea salt emission patterns from previous studies (Im et
28 al., 2012; Nabat et al., 2013; Rea et al., 2015; Liora et al., 2015).

29

30 5 Conclusions

31 In this work, satellite data from MODIS Terra (3/2000-12/2012) and Aqua (7/2002-12/2012)
32 were analyzed separately in order to examine the spatial and temporal variability of aerosols
33 over the region of Eastern Mediterranean. A high resolution ($0.1^\circ \times 0.1^\circ$) MODIS gridded



1 dataset was compiled using a method that could be used in future regional studies. A number
2 of tests were implemented and the dataset was validated in detail using sunphotometric
3 observations from 13 AERONET stations. It is shown that the gridding method we use offers
4 the best compromise for studying the spatial variability of aerosols on a regional or local
5 scale, preserving at the same time the representativeness of the real aerosol load over each
6 specific spot.

7 Based on MODIS observations the average AOD₅₅₀ levels over the region of Eastern
8 Mediterranean are $\sim 0.22 \pm 0.19$ which is $\sim 45\%$ higher than the global mean. A number of
9 aerosol hot spots that coincide with megacities, large and even medium size cities, industrial
10 zones, power plant complexes, river basins, etc., can be detected on the AOD maps. A
11 number of local aerosol sources can also be seen on satellite retrieved tropospheric NO₂ and
12 planetary boundary layer SO₂ maps from OMI/AURA. This is indicative of the strong
13 presence of anthropogenic aerosols over these regions. Topography and precipitation also
14 play an important role. Generally, regions with mountain ranges are characterized by low
15 AODs while regions of low altitude are characterized by higher AODs. Regions with high
16 AOD₅₅₀ are in many cases connected to low precipitation levels and vice versa as is the major
17 washout mechanism of atmospheric pollutants.

18 The AOD₅₅₀ patterns over Eastern Mediterranean exhibit a significant seasonal variability
19 which is mostly driven by precipitation, photochemical production of secondary organic
20 aerosols, transport of pollution and biomass burning aerosols from Central and Eastern
21 Europe and transport of dust from the Sahara Desert and the Middle East. Differences
22 between MODIS Terra and Aqua Collection 051 AOD₅₅₀ over the Eastern Mediterranean are
23 generally small ($\sim 8\%$ over land and $\sim 5\%$ over the sea). The comparison of the Terra-Aqua
24 differences with diurnal variabilities from the AERONET stations showed that only a part of
25 the observed differences is due to the diurnal variability of aerosols.

26 The MODIS data were combined with data from other satellites (Earth Probe TOMS,
27 OMI/AURA), reanalysis projects (ERA-Interim, MACC) and a chemistry-aerosol-transport
28 model (GOCART) to calculate the contribution of different types of aerosols to the total
29 AOD₅₅₀. The algorithm used was optimized for the Eastern Mediterranean through a number
30 of tests and comparison with LIVAS CALIOP/CALIPSO dust retrievals and AERONET
31 ground-based observations. A different approach is used for land and ocean covered areas as
32 there is not any reliable satellite retrieved quantity to separate the contribution of fine and
33 coarse mode aerosols over water surfaces.



1 Overall, for the land areas, based on MODIS Terra observations, 52 % (0.112 ± 0.087) of the
2 total AOD_{550} is due to anthropogenic aerosols, 32 % (0.074 ± 0.080) due to dust and 16 %
3 (0.034 ± 0.026) due to fine mode natural aerosols (see Fig. 7). For the oceanic areas, 41 %
4 (0.086 ± 0.085) of the total AOD_{550} is due to anthropogenic aerosols, 34 % (0.076 ± 0.185) due
5 to dust and 25 % (0.054 ± 0.018) due to marine aerosols. The results based on observations
6 from MODIS Aqua are in accord with previous studies.

7 Over land, the τ_a maxima are detected over local particle pollution sources (cities, industrial
8 zones, etc.). Over the sea, τ_a is higher along the coasts being significantly lower at greater
9 distance. Very high τ_d values appear over land regions in North Africa, Middle East, Anatolia
10 and oceanic areas across Eastern Mediterranean, especially for latitudes below 35°N . Over the
11 sea, dust loading exhibits two maxima, one at the coastal zone of Libya and one across the
12 coastal zone of the Middle East. τ_d decreases with distance from the large dust sources in the
13 South and South-East. Generally, dust reaches heights up to $\sim 4\text{-}5$ km in the area, the largest
14 fraction of dust mass being confined within the first 2-3 km of the troposphere. The spatial
15 variability of τ_n and τ_m is very low compared to τ_a and τ_d , following the total AOD_{550} patterns
16 and the near surface wind speed patterns, respectively.

17 Over land, the relative contribution of anthropogenic aerosols, dust and fine mode natural
18 aerosols to the total AOD_{550} exhibits a low seasonal variability, while over the sea the relative
19 contribution of anthropogenic aerosols, dust and marine aerosols shows a significant seasonal
20 variability.

21 τ_a nearly doubles during the warm period of the year (spring-summer), August and April
22 being the months with the highest τ_a levels. The summer peak is mostly the result of low
23 precipitation levels, enhancement of the photochemical production of secondary organic
24 aerosols and transport of pollution aerosols from Central Europe and biomass burning
25 aerosols from South-Western Russia and Eastern Europe during the biomass burning season
26 in July-August. The spring maximum in April is mostly the result of transport of biomass
27 burning aerosols from Russia in line with previous studies. Dust exhibits a strong peak in
28 spring (April), especially over the southern regions. April is the month with the highest τ_d
29 levels as a result of the high cyclonic activity over North Africa. The seasonal variability of
30 dust is much stronger and the spring maxima much more prominent over the sea as dust is
31 only occasionally transported there during episodic events, while over land, local sources
32 contribute to the dust burden, especially in summer due to the soil dryness. The seasonal
33 variability of fine mode natural aerosols is very low, the highest values appearing in spring



1 and summer. Marine aerosols also present a very low seasonal variability, the highest values
2 appearing in winter due to the high near surface wind speeds.
3 Overall, it is suggested that the AOD₅₅₀, τ_a , τ_d , τ_n and τ_m high resolution gridded dataset which
4 was compiled in this work could be used in a number of future atmospheric and biological
5 studies focusing on the region of Eastern Mediterranean (e.g. satellite and ground-based
6 studies on aerosol-cloud-radiation interactions, experimental and field campaign studies on
7 aerosols and clouds and research on the impact of aerosols on human health and nature). It is
8 also acknowledged that a future update of the results presented here using more recent
9 releases of MODIS aerosol data (e.g. Collection 6) and aerosol reanalysis datasets (e.g.
10 NASA's Modern-Era Retrospective Analysis For Research And Applications Aerosol Re-
11 analysis) would be a useful contribution.

12

13 **Acknowledgements**

14 This research received funding from the European Social Fund (ESF) and national resources
15 under the operational programme Education and Lifelong Learning (EdLL) within the
16 framework of the Action "Supporting Postdoctoral Researchers" (QUADIEEMS project),
17 from the European Research Council under the European Union's Seventh Framework
18 Programme (FP7/2007-2013)/ERC grant agreement no. 226144 (C8 project), from the FP7
19 Programme MarcoPolo (grant number 606953, theme SPA.2013.3.2-01) and from the
20 European Union's Horizon 2020 research and innovation programme under grant agreement
21 no. 654109. The authors express their gratitude to the teams that developed the algorithms and
22 produced the satellite products used in this study and to those who worked on the production
23 of the model and reanalysis data used here. Special thanks are expressed to NASA Goddard
24 Space Flight Center (GSFC) Level 1 and Atmosphere Archive and Distribution System
25 (LAADS) (<http://ladsweb.nascom.nasa.gov>) for making available the MODIS Terra and Aqua
26 Collection 051 level-2 aerosol data and the principal investigators and staff maintaining the
27 13 AERONET (<http://aeronet.gsfc.nasa.gov>) sites used in the present work. LIVAS has been
28 financed under the ESA-ESTEC project LIVAS (contract no. 4000104106/11/NL/FF/fk). We
29 thank the ICARE Data and Services Center (www.icare.univ-lille1.fr) for providing access to
30 NASA's CALIPSO data and acknowledge the use of NASA's CALIPSO data. Special thanks
31 are expressed to ECMWF (www.ecmwf.int) for the provision of the ERA-Interim and MACC
32 reanalysis data. NASA's GIOVANNI web database (<http://giovanni.gsfc.nasa.gov/giovanni/>)
33 is highly acknowledged for the provision of Aerosol Index data from Earth Probe TOMS and



1 OMI, aerosol data from the GOCART chemistry-aerosol-transport model (older version of
2 GIOVANNI), tropospheric NO₂ and PBL SO₂ columnar data from OMI and precipitation data
3 from 3B43 TRMM and Other Sources Monthly Rainfall Product. A.K.G. acknowledges the
4 fruitful discussions with various colleagues from the Max Planck Institute for Chemistry and
5 the Cyprus Institute (EEWRC) who indirectly contributed to this research.

6

7 **References**

8 Abdelkader, M., Metzger, S., Mamouri, R. E., Astitha, M., Barrie, L., Levin, Z., and
9 Lelieveld, J.: Dust-air pollution dynamics over the eastern Mediterranean, Atmos. Chem.
10 Phys., 15, 9173-9189, doi:10.5194/acp-15-9173-2015, 2015.

11 Acker, J. G. and Leptoukh, G.: Online analysis enhances use of NASA Earth science data,
12 Eos Trans. AGU, 88(2), 14-17, doi:10.1029/2007EO020003, 2007.

13 Alexandersson, H.: A homogeneity test applied to precipitation data, J. Climatol., 6(6), 661-
14 675, doi:10.1002/joc.3370060607, 1986.

15 Alexandri, G., Georgoulas, A. K., Zanis, P., Katragkou, E., Tsikerdekis, A., Kourtidis, K.,
16 and Meleti, C.: On the ability of RegCM4 regional climate model to simulate surface solar
17 radiation patterns over Europe: an assessment using satellite-based observations, Atmos.
18 Chem. Phys., 15, 13195-13216, doi:10.5194/acp-15-13195-2015, 2015.

19 Alpert, P. and Ganor, E.: Sahara mineral dust measurements from TOMS: Comparison to
20 surface observations over the Middle East for the extreme dust storm, 14-17 March 1998, J.
21 Geophys. Res., 106, D16, doi:10.1029/2000JD900366, 2001.

22 Antoine, D. and Nobileau, D.: Recent increase of Saharan dust transport over the
23 Mediterranean Sea, as revealed from ocean color satellite (SeaWiFS) observations, J.
24 Geophys. Res., 111, D12214, doi:10.1029/2005JD006795, 2006.

25 Amiridis V., Balis, D., Kazadzis, S., Giannakaki, E., Papayannis, A., and Zerefos, C.: Four
26 years aerosol observations with a Raman lidar at Thessaloniki, Greece, in the framework of
27 European Aerosol Research Lidar Network (EARLINET), J. Geophys. Res., 110, D21203,
28 doi:10.1029/2005JD006190, 2005.

29 Amiridis, V., Balis, D. S., Giannakaki, E., Stohl, A., Kazadzis, S., Koukouli, M. E., and
30 Zanis, P.: Optical characteristics of biomass burning aerosols over Southeastern Europe



- 1 determined from UVRaman lidar measurements, *Atmos. Chem. Phys.*, 9, 2431-2440,
2 doi:10.5194/acp-9-2431-2009, 2009.
- 3 Amiridis, V., Giannakaki, E., Balis, D. S., Gerasopoulos, E., Pytharoulis, I., Zanis, P.,
4 Kazadzis, S., Melas, D., and Zerefos, C.: Smoke injection heights from agricultural burning in
5 Eastern Europe as seen by CALIPSO, *Atmos. Chem. Phys.*, 10, 11567-11576,
6 doi:10.5194/acp-10-11567-2010, 2010.
- 7 Amiridis, V., Wandinger, U., Marinou, E., Giannakaki, E., Tsekeri, A., Basart, S., Kazadzis,
8 S., Gkikas, A., Taylor, M., Baldasano, J., and Ansmann, A.: Optimizing CALIPSO Saharan
9 dust retrievals, *Atmos. Chem. Phys.*, 13, 12089-12106, doi:10.5194/acp-13-12089-2013,
10 2013.
- 11 Amiridis, V., Marinou, E., Tsekeri, A., Wandinger, U., Schwarz, A., Giannakaki, E.,
12 Mamouri, R., Kokkalis, P., Biniotoglou, I., Solomos, S., Herekakis, T., Kazadzis, S.,
13 Gerasopoulos, E., Proestakis, E., Kottas, M., Balis, D., Papayannis, A., Kontoes, C.,
14 Kourtidis, K., Papagiannopoulos, N., Mona, L., Pappalardo, G., Le Rille, O., and Ansmann,
15 A.: LIVAS: a 3-D multi-wavelength aerosol/cloud database based on CALIPSO and
16 EARLINET, *Atmos. Chem. Phys.*, 15, 7127-7153, doi:10.5194/acp-15-7127-2015, 2015.
- 17 Athanassiou, G., Hatzianastassiou, N., Gkikas, A., Papadimas, C.D.: Estimating aerosol
18 optical depth over the broader greek area from MODIS satellite, *Water Air Soil. Pollut.*, 224
19 (7) doi:10.1007/S12270-013-1605-2, 2013
- 20 Balis, D., Amiridis, V., Nickovic, S., Papayannis, A., and Zerefos, C.: Optical properties of
21 Saharan dust layers as detected by a Raman lidar at Thessaloniki, Greece, *Geoph. Res. Lett.*,
22 31, doi:10.1029/2004GL019881, 2004.
- 23 Barnaba, F. and Gobbi, G. P.: Aerosol seasonal variability over the Mediterranean region and
24 relative impact of maritime, continental and Saharan dust particles over the basin from
25 MODIS data in the year 2001, *Atmos. Chem. Phys.*, 4, 2367-2391, doi:10.5194/acp-4-2367-
26 2004, 2004.
- 27 Basart, S., Pérez, C., Cuevas, E., Baldasano, J. M., and Gobbi, G. P.: Aerosol characterization
28 in Northern Africa, Northeastern Atlantic, Mediterranean Basin and Middle East from direct-
29 sun AERONET observations, *Atmos. Chem. Phys.*, 9, 8265-8282, doi:10.5194/acp-9-8265-
30 2009, 2009.



- 1 Bellouin, N., Jones, A., Haywood, J. and Christopher, S. A.: Updated estimate of aerosol
2 direct radiative forcing from satellite observations and comparison against the Hadley Centre
3 climate model, *J. Geophys. Res.*, 113(D10), D10205, doi:10.1029/2007JD009385, 2008.
- 4 Bellouin, N., Quaas, J., Morcrette, J.-J., and Boucher, O.: Estimates of aerosol radiative
5 forcing from the MACC re-analysis, *Atmos. Chem. Phys.*, 13, 2045-2062, doi:10.5194/acp-
6 13-2045-2013, 2013.
- 7 Benas, N., Hatzianastassiou, N., Matsoukas, C., Fotiadi, A., Mihalopoulos, N., and Vardavas,
8 I.: Aerosol shortwave direct radiative effect and forcing based on MODIS Level 2 data in the
9 Eastern Mediterranean (Crete), *Atmos. Chem. Phys.*, 11, 12647-12662, doi:10.5194/acp-11-
10 12647-2011, 2011.
- 11 Benas, N., Beloconi, A., and Chrysoulakis, N.: Estimation of urban PM10 concentration ,
12 based on MODIS and MERIS / AATSR synergistic observations, *Atmos. Environ.*, 79, 448-
13 454, doi:10.1016/j.atmosenv.2013.07.012, 2013.
- 14 Benedetti, A., Morcrette, J.-J., Boucher, O., Dethof, A., Engelen, R. J., Fisher, M., Flentjes,
15 H., Huneus, N., Jones, L., Kaiser, J. W., Kinne, S., Mangold, A., Razinger, M., Simmons, A.
16 J., Suttie, M., and the GEMS-AER team: Aerosol analysis and forecast in the ECMWF
17 Integrated Forecast System. Part II: Data assimilation, *J. Geophys. Res.*, 114, D13205,
18 doi:10.1029/2008JD011115, 2009.
- 19 Bergamo, A., Tafuro, A. M., Kinne, S., De Tomasi, F., and Perrone, M. R.: Monthly-averaged
20 anthropogenic aerosol direct radiative forcing over the Mediterranean based on AERONET
21 aerosol properties, *Atmos. Chem. Phys.*, 8, 6995-7014, doi:10.5194/acp-8-6995-2008, 2008.
- 22 Bucsela, E. J., Krotkov, N. A., Celarier, E. A., Lamsal, L. N., Swartz, W. H., Bhartia, P. K.,
23 Boersma, K. F., Veefkind, J. P., Gleason, J. F., and Pickering, K. E.: A new stratospheric and
24 tropospheric NO₂ retrieval algorithm for nadir-viewing satellite instruments: applications to
25 OMI, *Atmos. Meas. Tech.*, 6, 2607-2626, doi:10.5194/amt-6-2607-2013, 2013.
- 26 Burton, S. P., Ferrare, R. A., Vaughan, M. A., Omar, A. H., Rogers, R. R., Hostetler, C. A.,
27 and Hair, J. W.: Aerosol classification from airborne HSRL and comparisons with the
28 CALIPSO vertical feature mask, *Atmos. Meas. Tech.*, 6, 1397-1412, doi:10.5194/amt-6-
29 1397-2013, 2013.



- 1 Carmona, I. and Alpert, P.: Synoptic classification of Moderate Resolution Imaging
2 Spectroradiometer aerosols over Israel, *J. Geophys. Res.*, 114(D7), D07208,
3 doi:10.1029/2008JD010160, 2009.
- 4 Cesnulyte, V., Lindfors, A. V., Pitkänen, M. R. A., Lehtinen, K. E. J., Morcrette, J.-J., and
5 Arola, A.: Comparing ECMWF AOD with AERONET observations at visible and UV
6 wavelengths, *Atmos. Chem. Phys.*, 14, 593-608, doi:10.5194/acp-14-593-2014, 2014.
- 7 Chin, M., Rood, R. B., Lin, S.-J., Müller, J.-F. and Thompson, A. M.: Atmospheric sulfur
8 cycle simulated in the global model GOCART: Model description and global properties, *J.*
9 *Geophys. Res.*, 105(D20), 24671, doi:10.1029/2000JD900384, 2000.
- 10 Chin, M., Ginoux, P., Kinne, S., Torres, O., Holben, B. N., Duncan, B. N., Martin, R. V.,
11 Logan, J. A., Higurashi, A. and Nakajima, T.: Tropospheric Aerosol Optical Thickness from
12 the GOCART Model and Comparisons with Satellite and Sun Photometer Measurements, *J.*
13 *Atmos. Sci.*, 59(3), 461-483, doi:10.1175/1520-0469(2002)059<0461:TAOTFT>2.0.CO;2,
14 2002.
- 15 Chin, M., Chu, A., Levy, R., Remer, L., Kaufman, Y., Holben, B., Eck, T., Ginoux, P. and
16 Gao, Q.: Aerosol distribution in the Northern Hemisphere during ACE-Asia: Results from
17 global model, satellite observations, and Sun photometer measurements, *J. Geophys. Res.*
18 *Atmos.*, 109(D23), n/a-n/a, doi:10.1029/2004JD004829, 2004.
- 19 Chin, Mian, Diehl, T., Ginoux, P., and Malm, W.: Intercontinental transport of pollution and
20 dust aerosols: implications for regional air quality, *Atmos. Chem. Phys.*, 7, 5501-5517,
21 doi:10.5194/acp-7-5501-2007, 2007.
- 22 Chin, M., Diehl, T., Dubovik, O., Eck, T. F., Holben, B. N., Sinyuk, A., and Streets, D. G.:
23 Light absorption by pollution, dust, and biomass burning aerosols: a global model study and
24 evaluation with AERONET measurements, *Ann. Geophys.*, 27, 3439-3464,
25 doi:10.5194/angeo-27-3439-2009, 2009.
- 26 Chu, D. A., Kaufman, Y. J., Ichoku, C., Remer, L. A., Tanre, D., and Holben, B. N.:
27 Validation of MODIS aerosol optical depth retrieval over land. *Geophys. Res. Lett.*, 29, 8007,
28 doi:10.1029/2001GL013205, 2002.
- 29 Cuevas, E., Camino, C., Benedetti, A., Basart, S., Terradellas, E., Baldasano, J. M.,
30 Morcrette, J. J., Marticorena, B., Goloub, P., Mortier, A., Berjón, A., Hernández, Y., Gil-
31 Ojeda, M., and Schulz, M.: The MACC-II 2007-2008 reanalysis: atmospheric dust evaluation



- 1 and characterization over northern Africa and the Middle East, Atmos. Chem. Phys., 15,
2 3991-4024, doi:10.5194/acp-15-3991-2015, 2015.
- 3 De Meij, A. and Lelieveld, J.: Evaluating aerosol optical properties observed by ground-based
4 and satellite remote sensing over the Mediterranean and the Middle East in 2006, Atmos.
5 Res., 99(3-4), 415-433, doi:10.1016/j.atmosres.2010.11.005, 2011.
- 6 De Meij, A., Pozzer, A., Pringle, K. J., Tost, H., Lelieveld, J.: EMAC model evaluation and
7 analysis of atmospheric aerosol properties and distribution, Atmos. Res, 114-115, 38-69,
8 2012.
- 9 Dee, D. P., Uppala, S. M., Simmons, a. J., Berrisford, P., Poli, P., Kobayashi, S., Andrae, U.,
10 Balmaseda, M. a., Balsamo, G., Bauer, P., Bechtold, P., Beljaars, a. C. M., van de Berg, L.,
11 Bidlot, J., Bormann, N., Delsol, C., Dragani, R., Fuentes, M., Geer, a. J., Haimberger, L.,
12 Healy, S. B., Hersbach, H., Hólm, E. V., Isaksen, L., Kållberg, P., Köhler, M., Matricardi, M.,
13 McNally, a. P., Monge-Sanz, B. M., Morcrette, J. J., Park, B. K., Peubey, C., de Rosnay, P.,
14 Tavolato, C., Thépaut, J. N. and Vitart, F.: The ERA-Interim reanalysis: Configuration and
15 performance of the data assimilation system, Q. J. R. Meteorol. Soc., 137(656), 553-597,
16 doi:10.1002/qj.828, 2011.
- 17 Derimian, Y., Karnieli, A., Kaufman, Y. J., Andreae, M. O., Andreae, T. W., Dubovik, O.,
18 Maenhaut, W., Koren, I. and Holben, B. N.: Dust and pollution aerosols over the Negev
19 desert, Israel: Properties, transport, and radiative effect, J. Geophys. Res., 111(D5), D05205,
20 doi:10.1029/2005JD006549, 2006.
- 21 Dubovik, O., Smirnov, a., Holben, B. N., King, M. D., Kaufman, Y. J., Eck, T. F. and
22 Slutsker, I.: Accuracy assessments of aerosol optical properties retrieved from Aerosol
23 Robotic Network (AERONET) Sun and sky radiance measurements, J. Geophys. Res.,
24 105(D8), 9791, doi:10.1029/2000JD900040, 2000.
- 25 Dubovik, O. and King, M. D.: A flexible inversion algorithm for retrieval of aerosol optical
26 properties from Sun and sky radiance measurements, J. Geophys. Res., 105(D16), 20673,
27 doi:10.1029/2000JD900282, 2000.
- 28 Dubovik, O., Holben, B., Eck, T. F., Smirnov, A., Kaufman, Y. J., King, M. D., Tanré, D. and
29 Slutsker, I.: Variability of Absorption and Optical Properties of Key Aerosol Types Observed
30 in Worldwide Locations, J. Atmos. Sci., 59(3), 590-608, doi:10.1175/1520-
31 0469(2002)059<0590:VOAAOP>2.0.CO;2, 2002.



- 1 Eck, T. F., Holben, B. N., Reid, J. S., Dubovik, O., Smirnov, A., O'Neill, N. T., Slutsker, I.
2 and Kinne, S.: Wavelength dependence of the optical depth of biomass burning, urban, and
3 desert dust aerosols, *J. Geophys. Res.*, 104, 31333-31349, doi:10.1029/1999jd900923, 1999.
- 4 Elguindi, N., Clark, H., Ordóñez, C., Thouret, V., Flemming, J., Stein, O., Huijnen, V.,
5 Moinat, P., Inness, A., Peuch, V.-H., Stohl, A., Turquety, S., Athier, G., Cammas, J.-P., and
6 Schultz, M.: Current status of the ability of the GEMS/MACC models to reproduce the
7 tropospheric CO vertical distribution as measured by MOZAIC, *Geosci. Model Dev.*, 3, 501-
8 518, doi:10.5194/gmd-3-501-2010, 2010
- 9 El-Metwally, M., Alfaro, S. C., Abdel Wahab, M. M., Zakey, A. S., and Chatenet, B.:
10 Seasonal and inter-annual variability of the aerosol content in Cairo (Egypt) as deduced from
11 the comparison of MODIS aerosol retrievals with direct AERONET measurements, *Atmos.*
12 *Res.*, 97, 14-25, doi:10.1016/j.atmosres.2010.03.003, 2010.
- 13 El-Metwally, M. and Alfaro, S. C.: Correlation between meteorological conditions and
14 aerosol characteristics at an East-Mediterranean coastal site, *Atmos. Res.*, 132-133, 76-90,
15 doi:10.1016/j.atmosres.2013.05.006, 2013.
- 16 Flaounas, E., Kotroni, V., Lagouvardos, K., Kazadzis, S., Gkikas, A. and Hatzianastassiou,
17 N.: Cyclone contribution to dust transport over the Mediterranean region, *Atmos. Sci. Lett.*,
18 16(4), 473-478, doi:10.1002/asl.584, 2015.
- 19 Georgoulias, A. K., Balis, D., Koukouli, M. E., Meleti, C., Bais, A. and Zerefos, C.: A study
20 of the total atmospheric sulfur dioxide load using ground-based measurements and the
21 satellite derived Sulfur Dioxide Index, *Atmos. Environ.*, 43(9), 1693-1701,
22 doi:10.1016/j.atmosenv.2008.12.012, 2009.
- 23 Georgoulias, A. K. and Kourtidis, K. A.: On the aerosol weekly cycle spatiotemporal
24 variability over Europe, *Atmos. Chem. Phys.*, 11, 4611-4632, doi:10.5194/acp-11-4611-2011,
25 2011.
- 26 Georgoulias, A. K. and Kourtidis, K. A.: A high resolution satellite view of the aerosol
27 weekly cycle variability over Central Europe, *Atmos. Res.*, 107, 145-160,
28 doi:10.1016/j.atmosres.2012.01.003, 2012.
- 29 Georgoulias, A. K., Kourtidis, K. A., Kosmidis, E., Despotakis, T., and Symeonidis, P.:
30 AMFIC-WSDB: a web data base for hosting and easy retrieval of atmospheric data from
31 satellites, *Comput. Geosci.*, 48, 57-66, doi:10.1016/j.cageo.2012.05.001, 2012.



- 1 Georgoulas, A. K., Kourtidis, K. A., Alexandri, G., Rapsomanikis, S., and Sanchez-Lorenzo,
2 A.: Common summertime total cloud cover and aerosol optical depth weekly variabilities
3 over Europe: sign of the aerosol indirect effects?, *Atmos. Res.*, 153, 59-73,
4 doi:10.1016/j.atmosres.2014.07.031, 2015.
- 5 Gerasopoulos, E., Kokkalis, P., Amiridis, V., Liakakou, E., Perez, C., Haustein, K.,
6 Eleftheratos, K., Andreae, M. O., Andreae, T. W., and Zerefos, C. S.: Dust specific extinction
7 cross-sections over the Eastern Mediterranean using the BSC-DREAM model and sun
8 photometer data: the case of urban environments, *Ann. Geophys.*, 27, 2903-2912,
9 doi:10.5194/angeo-27-2903-2009, 2009.
- 10 Gerasopoulos, E., Amiridis, V., Kazadzis, S., Kokkalis, P., Eleftheratos, K., Andreae, M. O.,
11 Andreae, T. W., El-Askary, H., and Zerefos, C. S.: Three-year ground based measurements of
12 aerosol optical depth over the Eastern Mediterranean: the urban environment of Athens,
13 *Atmos. Chem. Phys.*, 11, 2145-2159, doi:10.5194/acp-11-2145-2011, 2011.
- 14 Ginoux, P., Chin, M., Tegen, I., Prospero, J. M., Holben, B., Dubovik, O. and Lin, S.-J.:
15 Sources and distributions of dust aerosols simulated with the GOCART model, *J. Geophys.*
16 *Res.*, 106(D17), 20255, doi:10.1029/2000JD000053, 2001.
- 17 Ginoux, P., Prospero, J., Torres, O. and Chin, M.: Long-term simulation of global dust
18 distribution with the GOCART model: correlation with North Atlantic Oscillation, *Environ.*
19 *Model. Softw.*, 19(2), 113-128, doi:10.1016/S1464-8152(03)00114-2, 2004.
- 20 Ginoux, P., Clarisse, L., Clerbaux, C., Coheur, P.-F., Dubovik, O., Hsu, N. C., and Van
21 Damme, M.: Mixing of dust and NH₃ observed globally over anthropogenic dust sources,
22 *Atmos. Chem. Phys.*, 12, 7351-7363, doi:10.5194/acp-12-7351-2012, 2012.
- 23 Giorgi, F.: Climate change hot-spots, *Geophys. Res. Lett.*, 33(8), 1-4,
24 doi:10.1029/2006GL025734, 2006.
- 25 Gkikas, A., Hatzianastassiou, N., and Mihalopoulos, N.: Aerosol events in the broader
26 Mediterranean basin based on 7-year (2000-2007) MODIS C005 data, *Ann. Geophys.*, 27,
27 3509-3522, doi:10.5194/angeo-27-3509-2009, 2009
- 28 Gkikas, A., Hatzianastassiou, N., Mihalopoulos, N., Katsoulis, V., Kazadzis, S., Pey, J.,
29 Querol, X., and Torres, O.: The regime of intense desert dust episodes in the Mediterranean
30 based on contemporary satellite observations and ground measurements, *Atmos. Chem. Phys.*,
31 13, 12135-12154, doi:10.5194/acp-13-12135-2013, 2013.



- 1 Gkikas, A., Houssos, E. E., Lolis, C. J., Bartzokas, A., Mihalopoulos, N., and
2 Hatzianastassiou, N.: Atmospheric circulation evolution related to desert-dust episodes over
3 the Mediterranean, *Q. J. Roy. Meteorol. Soc.*, 690, 1634-1645, 2014.
- 4 Hatzianastassiou, N., Gkikas, A., Mihalopoulos, N., Torres, O. and Katsoulis, B. D.: Natural
5 versus anthropogenic aerosols in the eastern Mediterranean basin derived from multiyear
6 TOMS and MODIS satellite data, *J. Geophys. Res. Atmos.*, 114(24),
7 doi:10.1029/2009JD011982, 2009.
- 8 Herman, J. R., Bhartia, P. K., Torres, O., Hsu, C., Seftor, C. and Celarier, E.: Global
9 distribution of UV-absorbing aerosols from Nimbus 7/TOMS data, *J. Geophys. Res. Atmos.*,
10 102(D14), 16911-16922, doi:10.1029/96JD03680, 1997.
- 11 Herrmann, M., Somot, S., Calmanti, S., Dubois, C., and Sevault, F.: Representation of spatial
12 and temporal variability of daily wind speed and of intense wind events over the
13 Mediterranean Sea using dynamical downscaling: impact of the regional climate model
14 configuration, *Nat. Hazards Earth Syst. Sci.*, 11, 1983-2001, doi:10.5194/nhess-11-1983-
15 2011, 2011.
- 16 Holben, B. N., Eck, T. F., Slutsker, I., Tanré, D., Buis, J. P., Setzer, A., Vermote, E., Reagan,
17 J. A., Kaufman, Y. J., Nakajima, T., Lavenue, F., Jankowiak, I. and Smirnov, A.:
18 AERONET—A Federated Instrument Network and Data Archive for Aerosol
19 Characterization, *Remote Sens. Environ.*, 66(1), 1-16, doi:10.1016/S0034-4257(98)00031-5,
20 1998.
- 21 Holben, B. N., Tanré, D., Smirnov, A., Eck, T. F., Slutsker, I., Abuhassan, N., Newcomb, W.
22 W., Schafer, J. S., Chatenet, B., Lavenue, F., Kaufman, Y. J., Castle, J. Vande, Setzer, A.,
23 Markham, B., Clark, D., Frouin, R., Halthore, R., Karneli, A., O'Neill, N. T., Pietras, C.,
24 Pinker, R. T., Voss, K. and Zibordi, G.: An emerging ground-based aerosol climatology:
25 Aerosol optical depth from AERONET, *J. Geophys. Res. Atmos.*, 106(D11), 12067-12097,
26 doi:10.1029/2001JD900014, 2001.
- 27 Hsu, N. C., Tsay, S. C., King, M. D. and Herman, J. R.: Aerosol properties over bright-
28 reflecting source regions, *IEEE Trans. Geosci. Remote Sens.*, 42(3), 557-569,
29 doi:10.1109/TGRS.2004.824067, 2004.



- 1 Hsu, N. C., Tsay, S. C., King, M. D. and Herman, J. R.: Deep Blue retrievals of Asian aerosol
2 properties during ACE-Asia, *IEEE Trans. Geosci. Remote Sens.*, 44(11), 3180-3195,
3 doi:10.1109/TGRS.2006.879540, 2006.
- 4 Hsu, N. C., Jeong, M.-J., Bettenhausen, C., Sayer, A. M., Hansell, R., Seftor, C. S., Huang, J.
5 and Tsay, S.-C.: Enhanced Deep Blue aerosol retrieval algorithm: The second generation, *J.*
6 *Geophys. Res. Atmos.*, 118(16), 9296-9315, doi:10.1002/jgrd.50712, 2013.
- 7 Huffman, G. J., Bolvin, D. T., Nelkin, E. J., Wolff, D. B., Adler, R. F., Gu, G., Hong, Y.,
8 Bowman, K. P., and Stocker, E. F.: The TRMM Multisatellite Precipitation Analysis
9 (TMPA): quasiglobal, multiyear, combined-sensor precipitation estimates at fine scales, *J.*
10 *Hydrometeorol.*, 8, 38-55, doi:10.1175/JHM560.1, 2007.
- 11 Husar, R. B., Prospero, J. M., and Stowe, L. L.: Characterization of tropospheric aerosols over
12 the oceans with the NOAA advanced very high resolution radiometer optical thickness
13 operational product, *J. Geophys. Res.*, 102, 16889-16909, 1997.
- 14 Ichoku, C.: A spatio-temporal approach for global validation and analysis of MODIS aerosol
15 products, *Geophys. Res. Lett.*, 29(12), 8006, doi:10.1029/2001GL013206, 2002.
- 16 Ichoku, C., Remer, L. A., and Eck, T. F.: Quantitative evaluation and intercomparison of
17 morning and afternoon Moderate Resolution Imaging Spectroradiometer (MODIS) aerosol
18 measurements from Terra and Aqua, *J. Geophys. Res.-Atmos.*, 110, D10S03,
19 doi:10.1029/2004JD004987, 2005.
- 20 Im, U., Markakis, K., Koçak, M., Gerasopoulos, E., Daskalakis, N., Mihalopoulos, N.,
21 Poupkou, A., Kındap, T., Unal, A. and Kanakidou, M.: Summertime aerosol chemical
22 composition in the Eastern Mediterranean and its sensitivity to temperature, *Atmos. Environ.*,
23 50, 164-173, doi:10.1016/j.atmosenv.2011.12.044, 2012.
- 24 Inness, A., Baier, F., Benedetti, A., Bouarar, I., Chabrillat, S., Clark, H., Clerbaux, C.,
25 Coheur, P., Engelen, R. J., Errera, Q., Flemming, J., George, M., Granier, C., Hadji-Lazaro,
26 J., Huijnen, V., Hurtmans, D., Jones, L., Kaiser, J. W., Kapsomenakis, J., Lefever, K., Leitão,
27 J., Razinger, M., Richter, A., Schultz, M. G., Simmons, A. J., Suttie, M., Stein, O., Thépaut,
28 J.-N., Thouret, V., Vrekoussis, M., Zerefos, C., and the MACC team: The MACC reanalysis:
29 an 8 yr data set of atmospheric composition, *Atmos. Chem. Phys.*, 13, 4073-4109,
30 doi:10.5194/acp-13-4073-2013, 2013.



- 1 Israelevich, P. L., Levin, Z., Joseph, J. H., and Ganor, E.: Desert aerosol transport in the
2 Mediterranean region as inferred from the TOMS aerosol index, *J. Geophys. Res.*, 107(D21),
3 4572, doi:10.1029/2001JD002011, 2002.
- 4 Israelevich, P. L., Ganor, E., Levin, Z., and Joseph, J. H.: Annual variations of physical
5 properties of desert dust over Israel, *J. Geophys. Res.*, 108(D13), 4381,
6 doi:10.1029/2002JD003163, 2003.
- 7 Israelevich, P., Ganor, E., Alpert, P., Kishcha, P. and Stupp, A.: Predominant transport paths
8 of Saharan dust over the Mediterranean Sea to Europe, *J. Geophys. Res.*, 117(D2), D02205,
9 doi:10.1029/2011JD016482, 2012.
- 10 Jones, T. A. and Christopher, S. A.: A reanalysis of MODIS fine mode fraction over ocean
11 using OMI and daily GOCART simulations, *Atmos. Chem. Phys.*, 11, 5805-5817,
12 doi:10.5194/acp-11-5805-2011, 2011.
- 13 Kabatas, B., Unal, A., Pierce, R. B., Kindap, T. and Pozzoli, L.: The contribution of Saharan
14 dust in PM10 concentration levels in Anatolian Peninsula of Turkey, *Sci. Total Environ.*, 488-
15 489(1), 413-421, doi:10.1016/j.scitotenv.2013.12.045, 2014.
- 16 Kalivitis, N., Gerasopoulos, E., Vrekoussis, M., Kouvarakis, G., Kubilay, N.,
17 Hatzianastassiou, N., Vardavas, I. and Mihalopoulos, N.: Dust transport over the eastern
18 Mediterranean derived from Total Ozone Mapping Spectrometer, Aerosol Robotic Network,
19 and surface measurements, *J. Geophys. Res.*, 112(D3), D03202, doi:10.1029/2006JD007510,
20 2007.
- 21 Kanakidou, M., Mihalopoulos, N., Kindap, T., Im, U., Vrekoussis, M., Gerasopoulos, E.,
22 Dermizaki, E., Unal, A., Koçak, M., Markakis, K., Melas, D., Kouvarakis, G., Youssef, A.
23 F., Richter, A., Hatzianastassiou, N., Hilboll, A., Ebojie, F., Wittrock, F., von Savigny, C.,
24 Burrows, J. P., Ladstaetter-Weissenmayer, A. and Moubasher, H.: Megacities as hot spots of
25 air pollution in the East Mediterranean, *Atmos. Environ.*, 45(6), 1223-1235,
26 doi:10.1016/j.atmosenv.2010.11.048, 2011.
- 27 Karnieli, A., Derimian, Y., Indoitu, R., Panov, N., Levy, R. C., Remer, L. A., Maenhaut, W.,
28 and Holben, B. N.: Temporal trend in anthropogenic sulfur aerosol transport from central and
29 eastern Europe to Israel, *J. Geophys. Res.*, 114, D00D19, doi:10.1029/2009JD011870, 2009.



- 1 Kaskaoutis, D. G., Kosmopoulos, P., Kambezidis, H. D. and Nastos, P. T.: Aerosol
2 climatology and discrimination of different types over Athens, Greece, based on MODIS data,
3 Atmos. Environ., 41(34), 7315-7329, doi:10.1016/j.atmosenv.2007.05.017, 2007.
- 4 Kaskaoutis, D. G., Kambezidis, H. D., Nastos, P. T. and Kosmopoulos, P. G.: Study on an
5 intense dust storm over Greece, Atmos. Environ., 42(29), 6884-6896,
6 doi:10.1016/j.atmosenv.2008.05.017, 2008.
- 7 Kaskaoutis, D. G., Nastos, P. T., Kosmopoulos, P. G. and Kambezidis, H. D.: The combined
8 use of satellite data, air-mass trajectories and model applications for monitoring dust transport
9 over Athens, Greece, Int. J. Remote Sens., 31(19), 5089-5109,
10 doi:10.1080/01431160903283868, 2010.
- 11 Kaskaoutis, D. G., Kharol, S. K., Sifakis, N., Nastos, P. T., Sharma, A. R., Badarinath, K. V.
12 S. and Kambezidis, H. D.: Satellite monitoring of the biomass-burning aerosols during the
13 wildfires of August 2007 in Greece: Climate implications, Atmos. Environ., 45(3), 716-726,
14 doi:10.1016/j.atmosenv.2010.09.043, 2011.
- 15 Kaskaoutis, D. G., Kosmopoulos, P. G., Nastos, P. T., Kambezidis, H. D., Sharma, M. and
16 Mehdi, W.: Transport pathways of Sahara dust over Athens, Greece as detected by MODIS
17 and TOMS, Geomatics, Nat. Hazards Risk, 3(1), 35-54, doi:10.1080/19475705.2011.574296,
18 2012a.
- 19 Kaskaoutis, D. G., Prasad, A. K., Kosmopoulos, P. G., Sinha, P. R., Kharol, S. K., Gupta, P.,
20 El-Askary, H. M. and Kafatos, M.: Synergistic use of remote sensing and modeling for
21 tracing dust storms in the mediterranean, Adv. Meteorol., 2012, doi:10.1155/2012/861026,
22 2012b.
- 23 Kaskaoutis, D. G., Nastos, P. T., Kosmopoulos, P. G. and Kambezidis, H. D.: Characterising
24 the long-range transport mechanisms of different aerosol types over Athens, Greece during
25 2000-2005, Int. J. Climatol., 32(8), 1249-1270, doi:10.1002/joc.2357, 2012c.
- 26 Kaskaoutis, D. G., Kahn, R. A., Pawan Gupta, P., Jayaraman, A., and Bartzokas, A.: Desert
27 Dust Properties, Modelling, and Monitoring, Advances in Meteorology, vol. 2012, ID
28 483632, 2 pp, 2012. doi:10.1155/2012/483632, 2012d.
- 29 Kaufman, Y. J., Tanré, D., Remer, L. a., Vermote, E. F., Chu, a. and Holben, B. N.:
30 Operational remote sensing of tropospheric aerosol over land from EOS moderate resolution



- 1 imaging spectroradiometer, *J. Geophys. Res.*, 102(D14), 17051, doi:10.1029/96JD03988,
2 1997.
- 3 Kaufman, Y. J., Koren, I., Remer, L. A., Tanré, D., Ginoux, P. and Fan, S.: Dust transport and
4 deposition observed from the Terra-Moderate Resolution Imaging Spectroradiometer
5 (MODIS) spacecraft over the Atlantic Ocean, *J. Geophys. Res. D Atmos.*, 110(10), 1-16,
6 doi:10.1029/2003JD004436, 2005.
- 7 Kazadzis, S., Bais, A., Amiridis, V., Balis, D., Meleti, C., Kouremeti, N., Zerefos, C. S.,
8 Rapsomanikis, S., Petrakakis, M., Kelesis, A., Tzoumaka, P., and Kelektoglou, K.: Nine
9 years of UV aerosol optical depth measurements at Thessaloniki, Greece, *Atmos. Chem.*
10 *Phys.*, 7, 2091-2101, doi:10.5194/acp-7-2091-2007, 2007.
- 11 Kazadzis, S., Veselovskii, I., Amiridis, V., Gröbner, J., Suvorina, A., Nyeki, S.,
12 Gerasopoulos, E., Kouremeti, N., Taylor, M., Tsekeri, A., and Wehrli, C.: Aerosol
13 microphysical retrievals from precision filter radiometer direct solar radiation measurements
14 and comparison with AERONET, *Atmos. Meas. Tech.*, 7, 2013-2025, doi:10.5194/amt-7-
15 2013-2014, 2014.
- 16 Kelektoglou, K. and Rapsomanikis, S.: AERONET observations of direct and indirect
17 aerosol effects over a South European conurbation, *Int. J. Remote Sens.*, 32, 2779-2798,
18 2011.
- 19 Khaliq, M. N. and Ouarda, T. B. M. J.: On the critical values of the standard normal
20 homogeneity test (SNHT), *Int. J. Climatol.*, 27(5), 681-687, doi:10.1002/joc.1438, 2007.
- 21 Kloog, I., Sorek-Hamer, M., Lyapustin, A., Coull, B., Wang, Y., Just, A. C., Schwartz, J., and
22 Broday, D. M.: Estimating daily PM_{2.5} and PM₁₀ across the complex geo-climate region of
23 Israel using MAIAC satellite-based AOD data, *Atmos. Environ.*, 122, 409-416,
24 doi:10.1016/j.atmosenv.2015.10.004, 2015.
- 25 Kokkalis, P., Papayannis, A., Amiridis, V., Mamouri, R. E., Veselovskii, I., Kolgotin, A.,
26 Tsaknakis, G., Kristiansen, N. I., Stohl, A., and Mona, L.: Optical, microphysical, mass and
27 geometrical properties of aged volcanic particles observed over Athens, Greece, during the
28 Eyjafjallajökull eruption in April 2010 through synergy of Raman lidar and sunphotometer
29 measurements, *Atmos. Chem. Phys.*, 13, 9303-9320, doi:10.5194/acp-13-9303-2013, 2013.
- 30 Koren, I., Joseph, J.H., Israelevich P.: Detection of dust plumes and their sources in
31 northeastern Libya, *Can J Remote Sens*, 29 (2003), pp. 792-796, 2003.



- 1 Kosmopoulos, P. G., Kaskaoutis, D. G., Nastos, P. T., and Kambezidis, H. D.: Seasonal
2 variation of columnar aerosol optical properties over Athens, Greece, based on MODIS data,
3 *Remote Sens. Environ.*, 112, 2354-2366, doi:10.1016/j.rse.2007.11.006, 2008.
- 4 Koukouli, M., Balis, D., Amiridis, V., Kazadzis, S., Bais, A., Nickovic, S. and Torres, O.:
5 Aerosol variability over Thessaloniki using ground based remote sensing observations and the
6 TOMS aerosol index, *Atmos. Environ.*, 40(28), 5367-5378,
7 doi:10.1016/j.atmosenv.2006.04.046, 2006.
- 8 Koukouli, M. E., Kazadzis, S., Amiridis, V., Ichoku, C., and Balis, D. S.: Comparisons of
9 satellite derived aerosol optical depth over a variety of sites in the southern Balkan region as
10 an indicator of local air quality, *Remote sensing of clouds and the atmosphere XII*, edited by:
11 Comerón, A., Picard, R. H., Schäfer, K., Slusser, J. R., and Amodeo, A., *Proceedings of SPIE*,
12 Vol. 67451V, doi:10.1117/12.737681, 2007.
- 13 Koukouli, M. E., Kazadzis, S., Amiridis, V., Ichoku, C., Balis, D. S. and Bais, A. F.: Signs of
14 a negative trend in the MODIS aerosol optical depth over the Southern Balkans, *Atmos.*
15 *Environ.*, 44(9), 1219-1228, doi:10.1016/j.atmosenv.2009.11.024, 2010.
- 16 Kourtidis, K., Rapsomanikis, S., Zerefos, C., Georgoulas, A. K., Pavlidou E.: Severe
17 particulate pollution from the deposition practices of the primary materials of a cement plant,
18 *Environ. Sci. Pollut. Res.*, 21, 9796-9808. doi:10.1007/S12356-014-2969-6, 2014.
- 19 Kourtidis, K., Stathopoulos, S., Georgoulas, A. K., Alexandri, G., and Rapsomanikis, S.: A
20 study of the impact of synoptic weather conditions and water vapor on aerosol-cloud
21 relationships over major urban clusters of China, *Atmos. Chem. Phys.*, 15, 10955-10964,
22 doi:10.5194/acp-15-10955-2015, 2015.
- 23 Kubilay, N.: Optical properties of mineral dust outbreaks over the northeastern
24 Mediterranean, *J. Geophys. Res.*, 108(D21), 4666, doi:10.1029/2003JD003798, 2003.
- 25 Lehahn, Y., Koren, I., Boss, E., Ben-Ami, Y., and Altaratz, O.: Estimating the maritime
26 component of aerosol optical depth and its dependency on surface wind speed using satellite
27 data, *Atmos. Chem. Phys.*, 10, 6711-6720, doi:10.5194/acp-10-6711-2010, 2010.
- 28 Lelieveld, J., Berresheim, H., Borrmann, S., Crutzen, P. J., Dentener, F. J., Fischer, H.,
29 Feichter, J., Flatau, P. J., Heland, J., Holzinger, R., Korrman, R., Lawrence, M. G., Levin,
30 Z., Markowicz, K. M., Mihalopoulos, N., Minikin, A., Ramanathan, V., De Reus, M.,
31 Roelofs, G. J., Scheeren, H. A., Sciare, J., Schlager, H., Schultz, M., Siegmund, P., Steil, B.,



- 1 Stephanou, E. G., Stier, P., Traub, M., Warneke, C., Williams, J. and Ziereis, H.: Global air
2 pollution crossroads over the Mediterranean., *Science*, 298(5594), 794-799,
3 doi:10.1126/science.1075457, 2002.
- 4 Levelt, P. F., Van den Oord, G. H. J., Dobber, M. R., Malkki, A., Visser, H., de Vries, J.,
5 Stammes, P., Lundell, J. O. V and Saari, H.: The Ozone Monitoring Instrument, *Ieee Trans.*
6 *Geosci. Remote Sens.*, 44(5), 1093-1101, doi:Urn:nbn:nl:ui:25-648485, 2006.
- 7 Levy, R. C.: Evaluation of the Moderate-Resolution Imaging Spectroradiometer (MODIS)
8 retrievals of dust aerosol over the ocean during PRIDE, *J. Geophys. Res.*, 108(D19), 8594,
9 doi:10.1029/2002JD002460, 2003.
- 10 Levy, R. C., Remer, L. A. and Dubovik, O.: Global aerosol optical properties and application
11 to Moderate Resolution Imaging Spectroradiometer aerosol retrieval over land, *J. Geophys.*
12 *Res. Atmos.*, 112(D13), doi:10.1029/2006JD007815, 2007a.
- 13 Levy, R. C., Remer, L. A., Mattoo, S., Vermote, E. F. and Kaufman, Y. J.: Second-generation
14 operational algorithm: Retrieval of aerosol properties over land from inversion of Moderate
15 Resolution Imaging Spectroradiometer spectral reflectance, *J. Geophys. Res. Atmos.*,
16 112(D13), doi:10.1029/2006JD007811, 2007b.
- 17 Levy, R., Remer, L., Tanré, D., Mattoo, S., and Kaufman, Y.: Algorithm for remote sensing
18 of tropospheric aerosol over dark targets from MODIS: Collections 005 and 051: Revision 2,
19 February 2009, MODIS Algorithm Theoretical Basis Document, 2009.
- 20 Levy, R. C., Remer, L. A., Kleidman, R. G., Mattoo, S., Ichoku, C., Kahn, R., and Eck, T. F.:
21 Global evaluation of the Collection 5 MODIS dark-target aerosol products over land, *Atmos.*
22 *Chem. Phys.*, 10, 10399-10420, doi:10.5194/acp-10-10399-2010, 2010.
- 23 Levy, R. C., Mattoo, S., Munchak, L. A., Remer, L. A., Sayer, A. M., Patadia, F., and Hsu, N.
24 C.: The Collection 6 MODIS aerosol products over land and ocean, *Atmos. Meas. Tech.*, 6,
25 2989-3034, doi:10.5194/amt-6-2989-2013, 2013.
- 26 Li, J., Carlson, B. E., and Laciš, A. A.: A study on the temporal and spatial variability of
27 absorbing aerosols using Total Ozone Mapping Spectrometer and Ozone Monitoring
28 Instrument Aerosol Index data, *J. Geophys. Res.*, 114(D9), D09213,
29 doi:10.1029/2008JD011278, 2009.



- 1 Li, C., Joiner, J., Krotkov, N. A., and Bhartia, P. K.: A fast and sensitive new satellite SO₂
2 retrieval algorithm based on principal component analysis: Application to the ozone
3 monitoring instrument, *Geophys. Res. Lett.*, 40, 6314-6318, doi:10.1002/2013GL058134,
4 2013.
- 5 Liora, N., Markakis, K., Poupkou, A., Giannaros, T. M. and Melas, D.: The natural emissions
6 model (NEMO): Description, application and model evaluation, *Atmos. Environ.*, 122, 493-
7 504, doi:10.1016/j.atmosenv.2015.10.014, 2015.
- 8 Lyapustin, A., Wang, Y., Xiong, X., Meister, G., Platnick, S., Levy, R., Franz, B., Korkin, S.,
9 Hilker, T., Tucker, J., Hall, F., Sellers, P., Wu, A., and Angal, A.: Scientific impact of
10 MODIS C5 calibration degradation and C6+ improvements, *Atmos. Meas. Tech.*, 7, 4353-
11 4365, doi:10.5194/amt-7-4353-2014, 2014.
- 12 Mamouri, R. E., Amiridis, V., Papayannis, A., Giannakaki, E., Tsaknakis, G., and Balis, D.
13 S.: Validation of CALIPSO space-borne-derived attenuated backscatter coefficient profiles
14 using a ground-based lidar in Athens, Greece, *Atmos. Meas. Tech.*, 2, 513-522,
15 doi:10.5194/amt-2-513-2009, 2009.
- 16 Mamouri, R. E., Ansmann, A., Nisantzi, A., Kokkalis, P., Schwarz, A., and Hadjimitsis, D.:
17 Low Arabian extinction-to-backscatter ratio, *Geophys. Res. Lett.*, 40, 4762-4766,
18 doi:10.1002/grl.50898, 2013.
- 19 Mamouri, R. E. and Ansmann, A.: Estimated desert-dust ice nuclei profiles from polarization
20 lidar: methodology and case studies, *Atmos. Chem. Phys.*, 15, 3463-3477, doi:10.5194/acp-
21 15-3463-2015, 2015.
- 22 Mangold, A., De Backer, H., De Paepe, B., Dewitte, S., Chiapello, I., Derimian, Y.,
23 Kacenelenbogen, M., Léon, J.-F., Huneeus, N., Schulz, M., Ceburnis, D., O'Dowd, C.,
24 Flentje, H., Kinne, S., Benedetti, A., Morcrette, J.-J. and Boucher, O.: Aerosol analysis and
25 forecast in the European Centre for Medium-Range Weather Forecasts Integrated Forecast
26 System: 3. Evaluation by means of case studies, *J. Geophys. Res.*, 116(D3), D03302,
27 doi:10.1029/2010JD014864, 2011.
- 28 Marey, H. S., Gille, J. C., El-Askary, H. M., Shalaby, E. A., and El-Raey, M. E.: Aerosol
29 climatology over Nile Delta based on MODIS, MISR and OMI satellite data, *Atmos. Chem.
30 Phys.*, 11, 10637-10648, doi:10.5194/acp-11-10637-2011, 2011.



- 1 Mateos, D., Antón, M., Toledano, C., Cachorro, V. E., Alados-Arboledas, L., Sorribas, M.,
2 Costa, M. J., and Baldasano, J. M.: Aerosol radiative effects in the ultraviolet, visible, and
3 near-infrared spectral ranges using long-term aerosol data series over the Iberian Peninsula,
4 Atmos. Chem. Phys., 14, 13497-13514, doi:10.5194/acp-14-13497-2014, 2014.
- 5 Mélin, F., Zibordi, G. and Djavidnia, S.: Development and validation of a technique for
6 merging satellite derived aerosol optical depth from SeaWiFS and MODIS, Remote Sens.
7 Environ., 108(4), 436-450, doi:10.1016/j.rse.2006.11.026, 2007.
- 8 Mishra, A. K., Klingmueller, K., Fredj, E., Lelieveld, J., Rudich, Y., and Koren, I.: Radiative
9 signature of absorbing aerosol over the eastern Mediterranean basin, Atmos. Chem. Phys., 14,
10 7213-7231, doi:10.5194/acp-14-7213-2014, 2014.
- 11 Morcrette, J.-J., Boucher, O., Jones, L., Salmond, D., Bechtold, P., Beljaars, A., Benedetti, A.,
12 Bonet, A., Kaiser, J. W., Razinger, M., Schulz, M., Serrar, S., Simmons, A. J., Sofiev, M.,
13 Suttie, M., Tompkins, A. M. and Untch, A.: Aerosol analysis and forecast in the European
14 Centre for Medium-Range Weather Forecasts Integrated Forecast System: Forward modeling,
15 J. Geophys. Res., 114(D6), D06206, doi:10.1029/2008JD011235, 2009.
- 16 Moulin, C., Lambert, C. E., Dayan, U., Masson, V., Ramonet, M., Bousquet, P., Legrand, M.,
17 Balkanski, Y. J., Guelle, W., Marticorena, B., Bergametti, G. and Dulac, F.: Satellite
18 climatology of African dust transport in the Mediterranean atmosphere, J. Geophys. Res.
19 Atmos., 103(D11), 13137-13144, doi:10.1029/98JD00171, 1998.
- 20 Nabat, P., Solmon, F., Mallet, M., Kok, J. F., and Somot, S.: Dust emission size distribution
21 impact on aerosol budget and radiative forcing over the Mediterranean region: a regional
22 climate model approach, Atmos. Chem. Phys., 12, 10545-10567, doi:10.5194/acp-12-10545-
23 2012, 2012.
- 24 Nabat, P., Somot, S., Mallet, M., Chiapello, I., Morcrette, J. J., Solmon, F., Szopa, S., Dulac,
25 F., Collins, W., Ghan, S., Horowitz, L. W., Lamarque, J. F., Lee, Y. H., Naik, V., Nagashima,
26 T., Shindell, D., and Skeie, R.: A 4-D climatology (1979-2009) of the monthly tropospheric
27 aerosol optical depth distribution over the Mediterranean region from a comparative
28 evaluation and blending of remote sensing and model products, Atmos. Meas. Tech., 6, 1287-
29 1314, doi:10.5194/amt-6-1287-2013, 2013.



- 1 Nikitidou, E. and Kazantzidis, A.: On the differences of ultraviolet and visible irradiance
2 calculations in the Mediterranean basin due to model- and satellite-derived climatologies of
3 aerosol optical properties, *Int. J. Climatol.*, 33(13), 2877-2888, doi:10.1002/joc.3638, 2013.
- 4 Nisantzi, A., Mamouri, R. E., Ansmann, A., Schuster, G. L., and Hadjimitsis, D. G.: Middle
5 East versus Saharan dust extinction-to-backscatter ratios, *Atmos. Chem. Phys.*, 15, 7071-
6 7084, doi:10.5194/acp-15-7071-2015, 2015.
- 7 Papadimas, C. D., Hatzianastassiou, N., Mihalopoulos, N., Querol, X., and Vardavas, I.:
8 Spatial and temporal variability in aerosol properties over the Mediterranean basin based on
9 6-year (2000-2006) MODIS data, *J. Geophys. Res.*, 113(D11), D11205,
10 doi:10.1029/2007JD009189, 2008.
- 11 Papadimas, C. D., Hatzianastassiou, N., Mihalopoulos, N., Kanakidou, M., Katsoulis, B. D.,
12 and Vardavas, I.: Assessment of the MODIS Collections C005 and C004 aerosol optical depth
13 products over the Mediterranean basin, *Atmos. Chem. Phys.*, 9, 2987-2999, doi:10.5194/acp-
14 9-2987-2009, 2009.
- 15 Papadimas, C. D., Hatzianastassiou, N., Matsoukas, C., Kanakidou, M., Mihalopoulos, N. and
16 Vardavas, I.: The direct effect of aerosols on solar radiation over the broader Mediterranean
17 basin, *Atmos. Chem. Phys.*, 12(15), 7165-7185, doi:10.5194/acp-12-7165-2012, 2012.
- 18 Papayannis, A. and Balis, D.: Study of the structure of the lower troposphere over Athens
19 using a backscattering Lidar during the MEDCAPHOT-TRACE experiment: Measurements
20 over a suburban area, *Atmos. Envi.*, 32, 12, 2161-2172, 1998.
- 21 Papayannis, A., Balis, D., Amiridis, V., Chourdakis, G., Tsaknakis, G., Zerefos, C., Castanho,
22 A. D. A., Nickovic, S., Kazadzis, S., and Grabowski, J.: Measurements of Saharan dust
23 aerosols over the Eastern Mediterranean using elastic backscatter-Raman lidar,
24 spectrophotometric and satellite observations in the frame of the EARLINET project, *Atmos.*
25 *Chem. Phys.*, 5, 2065-2079, doi:10.5194/acp-5-2065-2005, 2005.
- 26 Papayannis, A., Mamouri, R. E., Amiridis, V., Kazadzis, S., Pérez, C., Tsaknakis, G.,
27 Kokkalis, P., and Baldasano, J. M.: Systematic lidar observations of Saharan dust layers over
28 Athens, Greece in the frame of EARLINET project (2004-2006), *Ann. Geophys.*, 27, 3611-
29 3620, doi:10.5194/angeo-27-3611-2009, 2009.
- 30 Pey, J., Querol, X., Alastuey, A., Forastiere, F., and Stafoggia, M.: African dust outbreaks
31 over the Mediterranean Basin during 2001-2011: PM10 concentrations, phenomenology and



- 1 trends, and its relation with synoptic and mesoscale meteorology, *Atmos. Chem. Phys.*, 13,
2 1395-1410, doi:10.5194/acp-13-1395-2013, 2013.
- 3 Pozzer, A., de Meij, A., Yoon, J., Tost, H., Georgoulias, A. K., and Astitha, M.: AOD trends
4 during 2001–2010 from observations and model simulations, *Atmos. Chem. Phys.*, 15, 5521-
5 5535, doi:10.5194/acp-15-5521-2015, 2015.
- 6 Rea, G., Turquety, S., Menut, L., Briant, R., Mailler, S., and Siour, G.: Source contributions
7 to 2012 summertime aerosols in the Euro-Mediterranean region, *Atmos. Chem. Phys.*, 15,
8 8013-8036, doi:10.5194/acp-15-8013-2015, 2015.
- 9 Remer, L. A., Tanre, D., Kaufman, Y. J., Ichoku, C., Mattoo, S., Levy, R., Chu, D. A.,
10 Holben, B., Dubovik, O., Smirnov, A., Martins, J. V., Li, R. R., Ahmad, Z.: Validation of
11 MODIS aerosol retrieval over ocean, *Geophys. Res. Lett.*, 29(12), 2-5,
12 doi:10.1029/2001GL013204, 2002.
- 13 Remer, L. A., Kaufman, Y. J., Tanré, D., Mattoo, S., Chu, D. A., Martins, J. V., Li, R.-R.,
14 Ichoku, C., Levy, R. C., Kleidman, R. G., Eck, T. F., Vermote, E. and Holben, B. N.: The
15 MODIS Aerosol Algorithm, Products, and Validation, *J. Atmos. Sci.*, 62(4), 947-973,
16 doi:10.1175/JAS3385.1, 2005.
- 17 Remer, L. A., Tanré, D., Kaufman, Y. J., Levy, R., and Mattoo, S.: Algorithm for remote
18 sensing of Tropospheric aerosol from MODIS: Collection 5, Product ID: MOD04/MYD04,
19 2006.
- 20 Remer, L. A., Kleidman, R. G., Levy, R. C., Kaufman, Y. J., Tanré, D., Mattoo, S., Martins,
21 J. V., Ichoku, C., Koren, I., Yu, H. and Holben, B. N.: Global aerosol climatology from the
22 MODIS satellite sensors, *J. Geophys. Res.*, 113(D14), D14S07, doi:10.1029/2007JD009661,
23 2008.
- 24 Retalis, A. and Sifakis, N.: Urban aerosol mapping over Athens using the differential textural
25 analysis (DTA) algorithm on MERIS-ENVISAT data, *ISPRS J. Photogramm. Remote Sens.*,
26 65(1), 17-25, doi:10.1016/j.isprsjprs.2009.08.001, 2010.
- 27 Rudich, Y., Kaufman, Y. J., Dayan, U., Yu, H., and Kleidman, R. G.: Estimation of
28 transboundary transport of pollution aerosols by remote sensing in the eastern Mediterranean,
29 *J. Geophys. Res.*, 113, D14S14, doi:10.1029/2007JD009601, 2008.



- 1 Sayer, A. M., Hsu, N. C., Bettenhausen, C. and Jeong, M. J.: Validation and uncertainty
2 estimates for MODIS Collection 6 “deep Blue” aerosol data, *J. Geophys. Res. Atmos.*,
3 118(14), 7864-7872, doi:10.1002/jgrd.50600, 2013.
- 4 Sayer, A. M., Munchak, L. A., Hsu, N. C., Levy, R. C., Bettenhausen, C. and Jeong, M.-J.:
5 MODIS Collection 6 aerosol products: Comparison between Aqua’s e-Deep Blue, Dark
6 Target, and “merged” data sets, and usage recommendations, *J. Geophys. Res. Atmos.*,
7 119(24), 13,965-13,989, doi:10.1002/2014JD022453, 2014.
- 8 Sciare, J., Oikonomou, K., Favez, O., Liakakou, E., Markaki, Z., Cachier, H., and
9 Mihalopoulos, N.: Long-term measurements of carbonaceous aerosols in the Eastern
10 Mediterranean: evidence of long-range transport of biomass burning, *Atmos. Chem. Phys.*, 8,
11 5551-5563, doi:10.5194/acp-8-5551-2008, 2008.
- 12 Shi, Y., Zhang, J., Reid, J. S., Holben, B., Hyer, E. J., and Curtis, C.: An analysis of the
13 collection 5 MODIS over-ocean aerosol optical depth product for its implication in aerosol
14 assimilation, *Atmos. Chem. Phys.*, 11, 557-565, doi:10.5194/acp-11-557-2011, 2011.
- 15 Shi, Y., Zhang, J., Reid, J. S., Hyer, E. J., and Hsu, N. C.: Critical evaluation of the MODIS
16 Deep Blue aerosol optical depth product for data assimilation over North Africa, *Atmos.*
17 *Meas. Tech.*, 6, 949-969, doi:10.5194/amt-6-949-2013, 2013.
- 18 Sifakis, N. I., Iossifidis, C. and Kontoes, C.: CHRISTINE Code for High ResolutIon Satellite
19 mapping of optical ThIckness and Ångstrom Exponent. Part II: First application to the urban
20 area of Athens, Greece and comparison to results from previous contrast-reduction codes,
21 *Comput. Geosci.*, 62, 142-149, doi:10.1016/j.cageo.2013.05.011, 2014.
- 22 Smirnov, A.: Maritime component in aerosol optical models derived from Aerosol Robotic
23 Network data, *J. Geophys. Res.*, 108(D1), 4033, doi:10.1029/2002JD002701, 2003.
- 24 Sorek-Hamer, M., Cohen, A., Levy, R. C., Ziv, B. and Broday, D. M.: Classification of dust
25 days by satellite remotely sensed aerosol products, *Int. J. Remote Sens.*, 34(8), 2672-2688,
26 doi:10.1080/01431161.2012.748991, 2013.
- 27 Tanré, D., Kaufman, Y. J., Herman, M. and Mattoo, S.: Remote sensing of aerosol properties
28 over oceans using the MODIS/EOS spectral radiances, *J. Geophys. Res. Atmos.*, 102(D14),
29 16971-16988, doi:10.1029/96JD03437, 1997.



- 1 Tsaknakis, G., Papayannis, A., Kokkalis, P., Amiridis, V., Kambezidis, H. D., Mamouri, R.
2 E., Georgoussis, G., and Avdikos, G.: Inter-comparison of lidar and ceilometer retrievals for
3 aerosol and Planetary Boundary Layer profiling over Athens, Greece, *Atmos. Meas. Tech.*, 4,
4 1261-1273, doi:10.5194/amt-4-1261-2011, 2011.
- 5 Tyrllis, E. and Lelieveld, J.: Climatology and dynamics of the summer Etesian winds over the
6 Eastern Mediterranean, *J. Atmos. Sci.*, 70, 3374-3396, doi:10.1175/JAS-D-13-035.1, 2013.
- 7 Varga, G., Ujvari, G., and Kovacs, J.: Spatiotemporal patterns of Saharan dust outbreaks in
8 the Mediterranean Basin, *Aeolian Res.*, 15, 151-160, doi:10.1016/j.aeolia.2014.06.005, 2014.
- 9 Vrekoussis, M., Liakakou, E., Koçak, M., Kubilay, N., Oikonomou, K., Sciare, J. and
10 Mihalopoulos, N.: Seasonal variability of optical properties of aerosols in the Eastern
11 Mediterranean, *Atmos. Environ.*, 39(37), 7083-7094, doi:10.1016/j.atmosenv.2005.08.011,
12 2005.
- 13 Zyrichidou, I., Koukouli, M. E., Balis, D. S., Katragkou, E., Melas, D., Poupkou, A.,
14 Kioutsioukis, I., van der A, R., Boersma, F. K., van Roozendaal, M., and Richter, A.: Satellite
15 observations and model simulations of tropospheric NO₂ columns over south-eastern Europe,
16 *Atmos. Chem. Phys.*, 9, 6119-6134, doi:10.5194/acp-9-6119-2009, 2009.
- 17
18
19
20
21
22
23
24
25
26
27
28
29
30
31
32



1 **Table 1.** Full name, abbreviation, geolocation, host country and type of the 13 AERONET
 2 cimel sunphotometer sites used for the validation of MODIS Terra and Aqua Collection 051
 3 observations. The common measurement period of MODIS and AERONET data and the
 4 corresponding overpass time of MODIS Terra and Aqua (Italics) over each station are also
 5 given.

6

| AERONET Station | Lat (°N) | Lon (°E) | Period of study | Country | Type | TERRA overpass | AQUA overpass |
|---------------------------|----------|----------|-----------------|-------------|---------------------|----------------|-----------------------|
| ATHENS-NOA (ATH) | 37.988 | 23.775 | 05/2008-10/2012 | Greece | Urban (coastal) | 9:23±22min UT | <i>11:32±22min UT</i> |
| Bucharest Inoe (BUC) | 44.348 | 26.030 | 07/2007-09/2012 | Romania | Sub-urban (coastal) | 9:17±24min UT | <i>11:15±20min UT</i> |
| CUT-TEPAK (CUT) | 34.675 | 33.043 | 04/2010-12/2012 | Cyprus | Urban (coastal) | 8:43±25min UT | <i>10:55±25min UT</i> |
| Eforie (EFO) | 44.075 | 28.632 | 09/2009/12/2012 | Romania | Rural (coastal) | 9:09±21min UT | <i>11:04±21min UT</i> |
| FORTH Crete (FOR) | 35.333 | 25.282 | 01/2003-08/2011 | Greece | Rural (coastal) | 9:12±24min UT | <i>11:25±25min UT</i> |
| IMS-METU-ERDEMLI (IMS) | 36.565 | 34.255 | 01/2004-01/2012 | Turkey | Rural (coastal) | 8:39±23min UT | <i>10:48±22min UT</i> |
| Lecce University (LEC) | 40.335 | 18.111 | 03/2003-12/2012 | Italy | Sub-urban (coastal) | 9:44±25min UT | <i>11:49±25min UT</i> |
| Nes ziona (NES) | 31.922 | 34.789 | 02/2000-12/2012 | Israel | Sub-urban (coastal) | 8:38±24min UT | <i>10:44±25min UT</i> |
| SEDE BOKER (SED) | 30.855 | 34.782 | 01/2000-04/2012 | Israel | Rural (semi-arid) | 8:30±27min UT | <i>10:50±25min UT</i> |
| Sevastopol (SEV) | 44.616 | 33.517 | 05/2006-12/2012 | Ukr.-Crimea | Urban (coastal) | 8:51±21min UT | <i>10:40±21min UT</i> |
| Thessaloniki (THE) | 40.630 | 22.960 | 09/2005-12/2012 | Greece | Urban (coastal) | 9:28±25min UT | <i>11:32±22min UT</i> |
| TUBITAK UZAY Ankara (TUB) | 39.891 | 32.778 | 12/2009-04/2012 | Turkey | Urban (continental) | 8:48±26min UT | <i>10:56±24min UT</i> |
| Xanthi (XAN) | 41.147 | 24.919 | 01/2008-10/2010 | Greece | Rural (coastal) | 9:18±25min UT | <i>11:24±21min UT</i> |

7

8

9

10

11

12

13

14

15

16

17

18

19

20

21

22

23

24

25

26

27



1 **Table 2.** Results of the comparison of spatially (using a spatial window around each station)
 2 and temporally (± 30 min from the MODIS overpass time) collocated MODIS Terra and Aqua
 3 (Italics) Collection 051 level-2 and AERONET sunphotometric (quadratically interpolated)
 4 AOD₅₅₀ observations for the Eastern Mediterranean stations. The algorithms used for the
 5 production of the validated MODIS data (DT and DB), the spatial window used for the spatial
 6 collocation (25 x 25 km² or 50 x 50 km² window around each station) with the AERONET
 7 data, the average MODIS and AERONET AOD₅₅₀ and the corresponding $\pm 1\sigma$ values, the
 8 mean difference between them, the normalized mean bias (NMB) and the corresponding root
 9 mean squared (RMS) error, the percentage of the collocation points that fall within the
 10 expected error (EE) envelope and the pre-launch expected error (plEE) envelope (Expected
 11 Uncertainty - EU envelope for DB data), the correlation coefficient R, the slope a and the
 12 intercept of the regression line and the number of the collocation points are given in the table.
 13 L10 denotes the use of a collocation window of 50° x 50° as in Levy et al. (2010) while HQ
 14 denotes the use of high quality data only.

15

| Alg. | Window | MODIS TERRA MODIS AQUA | AERONET | Mean Diff. | NMB % | RMS err. | in EE % | in plEE % | R | a | b | Obs |
|------------------------|--------------------|---------------------------|--------------------|--------------------|--------------|-------------|--------------|--------------|-------------|--------------|--------------|-------------|
| DT | 25 km | 0.223±0.163 | 0.200±0.123 | 0.023±0.106 | 11.59 | 0.11 | 63.28 | 67.78 | 0.76 | 1.007 | 0.022 | 6697 |
| <i>DT</i> | <i>25 km</i> | <i>0.247±0.173</i> | <i>0.197±0.121</i> | <i>0.050±0.109</i> | <i>25.18</i> | <i>0.12</i> | <i>57.14</i> | <i>61.87</i> | <i>0.78</i> | <i>1.113</i> | <i>0.027</i> | <i>6283</i> |
| DT | 50 km (L10) | 0.204±0.152 | 0.194±0.124 | 0.010±0.085 | 5.10 | 0.09 | 70.17 | 74.64 | 0.83 | 1.016 | 0.007 | 6054 |
| <i>DT</i> | <i>50 km (L10)</i> | <i>0.224±0.155</i> | <i>0.194±0.125</i> | <i>0.030±0.088</i> | <i>15.34</i> | <i>0.09</i> | <i>66.76</i> | <i>70.45</i> | <i>0.82</i> | <i>1.018</i> | <i>0.026</i> | <i>5557</i> |
| DB | 25 km | 0.226±0.177 | 0.186±0.128 | 0.040±0.162 | 21.38 | 0.17 | - | 51.90 | 0.47 | 0.657 | 0.104 | 2580 |
| <i>DB</i> | <i>25 km</i> | <i>0.242±0.217</i> | <i>0.182±0.118</i> | <i>0.06±0.196</i> | <i>33.03</i> | <i>0.20</i> | - | <i>55.30</i> | <i>0.44</i> | <i>0.815</i> | <i>0.094</i> | <i>5345</i> |
| DB _{HQ} | 25 km | 0.229±0.158 | 0.186±0.132 | 0.043±0.141 | 22.82 | 0.15 | - | 52.41 | 0.54 | 0.651 | 0.108 | 498 |
| <i>DB_{HQ}</i> | <i>25 km</i> | <i>0.260±0.220</i> | <i>0.186±0.138</i> | <i>0.074±0.204</i> | <i>39.84</i> | <i>0.22</i> | - | <i>52.34</i> | <i>0.42</i> | <i>0.670</i> | <i>0.136</i> | <i>896</i> |

16

17

18

19

20

21

22

23

24

25

26

27

28

29



1 **Table 3.** AOD₅₅₀ levels, the corresponding $\pm 1\sigma$ values and the number of gridded values used
 2 for the calculations over Eastern Mediterranean (EMT), over the land covered part (EML),
 3 over the oceanic part and over the 9 sub-regions of Eastern Mediterranean appearing in Fig. 1
 4 based on the MODIS Terra and Aqua (Italics) observations.

| Region | MODIS TERRA AOD ₅₅₀ | Num. of values | MODIS AQUA AOD ₅₅₀ | Num. of values |
|--------|-----------------------------------|----------------|----------------------------------|-----------------|
| EMT | 0.215±0.187 | 61496654 | <i>0.217±0.199</i> | <i>49522934</i> |
| EML | 0.219±0.165 | 25923766 | <i>0.239±0.189</i> | <i>21008713</i> |
| EMO | 0.213±0.201 | 35572888 | <i>0.202±0.205</i> | <i>28514221</i> |
| NBL | 0.183±0.163 | 5563495 | <i>0.187±0.162</i> | <i>3853688</i> |
| SBL | 0.197±0.152 | 7345829 | <i>0.207±0.152</i> | <i>5272449</i> |
| ANL | 0.223±0.146 | 7948817 | <i>0.228±0.148</i> | <i>5539261</i> |
| NAL | 0.282±0.192 | 5065625 | <i>0.306±0.238</i> | <i>6343315</i> |
| BSO | 0.198±0.150 | 6433951 | <i>0.183±0.134</i> | <i>5262438</i> |
| NWO | 0.209±0.162 | 11645069 | <i>0.197±0.154</i> | <i>9231630</i> |
| SWO | 0.226±0.266 | 6202893 | <i>0.223±0.310</i> | <i>4925665</i> |
| NEO | 0.214±0.196 | 4807910 | <i>0.199±0.166</i> | <i>3896554</i> |
| SEO | 0.221±0.236 | 6483065 | <i>0.210±0.239</i> | <i>5197934</i> |

6

7

8

9

10

11

12

13

14

15

16

17

18

19

20

21

22

23

24

25

26

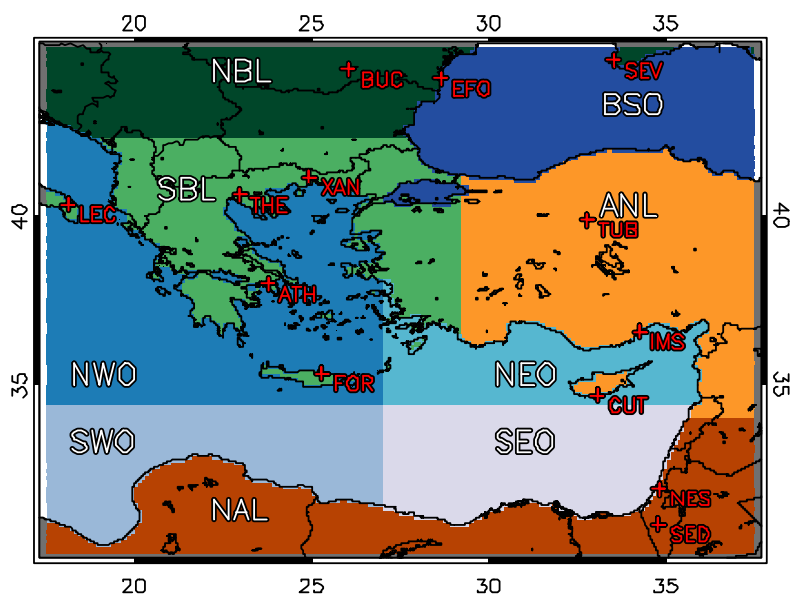
27



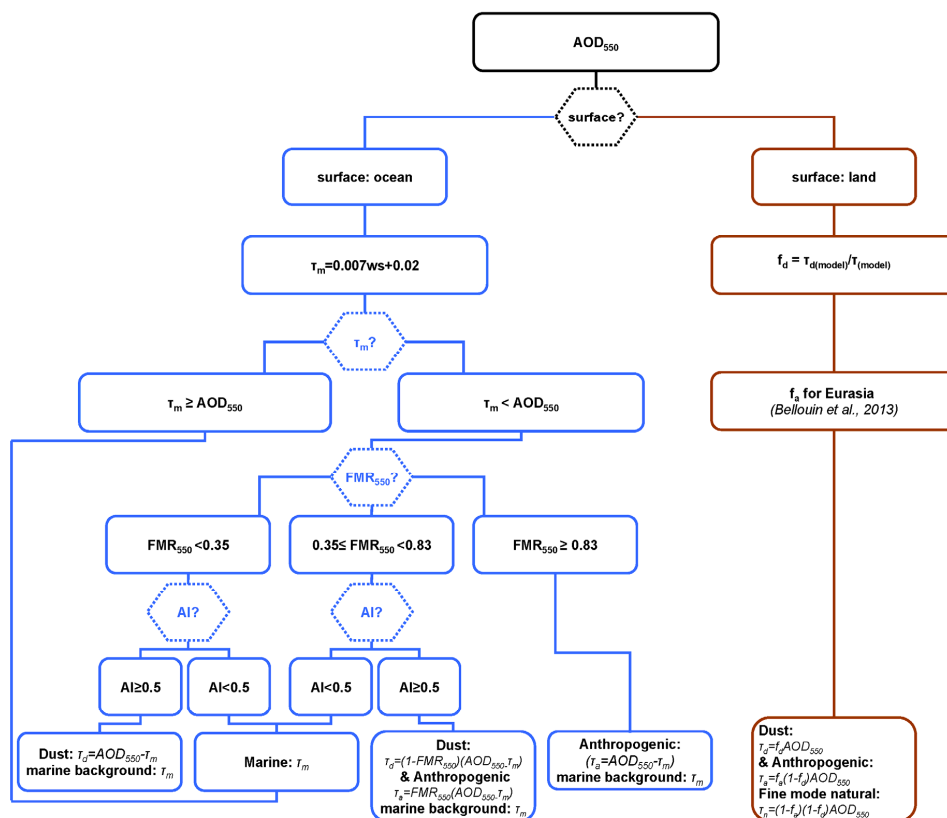
1 **Table 4.** Relative contribution of anthropogenic aerosols, dust, fine mode natural and marine
 2 aerosols to the total AOD₅₅₀ (bold) and the corresponding τ_a , τ_d , τ_n , τ_m levels with their $\pm 1\sigma$
 3 values (in parentheses) over Eastern Mediterranean (EMT), over the land covered part (EML),
 4 over the oceanic part and over the 9 sub-regions of Eastern Mediterranean appearing in Fig. 1
 5 based on the MODIS Terra and Aqua (Italics) observations. The sum of the aerosol type
 6 AODs per region does not necessarily correspond to the total AOD₅₅₀ values appearing in
 7 Table 3 as these results were for the total of the days with aerosol retrievals even for days
 8 when our aerosol type separation algorithm was not applicable.

| Region | Satellite | Contribution to MODIS TERRA/AQUA AOD ₅₅₀ | | | |
|--------|-----------|---|---------------------------|---------------------------|---------------------------|
| | | Anthropogenic | Dust | Fine mode natural | Marine |
| EML | TERRA | 52 % (0.112±0.087) | 32 % (0.074±0.080) | 16 % (0.034±0.026) | - |
| | AQUA | 50 % (0.117±0.093) | 35 % (0.090±0.102) | 15 % (0.035±0.028) | - |
| EMO | TERRA | 41 % (0.086±0.085) | 34 % (0.076±0.185) | - | 25 % (0.054±0.018) |
| | AQUA | 40 % (0.079±0.080) | 33 % (0.070±0.181) | - | 27 % (0.054±0.018) |
| NBL | TERRA | 59 % (0.108±0.101) | 23 % (0.042±0.046) | 18 % (0.032±0.030) | - |
| | AQUA | 59 % (0.110±0.100) | 24 % (0.045±0.047) | 17 % (0.033±0.030) | - |
| SBL | TERRA | 55 % (0.109±0.088) | 28 % (0.056±0.058) | 17 % (0.033±0.026) | - |
| | AQUA | 55 % (0.113±0.088) | 29 % (0.060±0.060) | 16 % (0.034±0.026) | - |
| ANL | TERRA | 51 % (0.113±0.075) | 34 % (0.076±0.068) | 15 % (0.034±0.023) | - |
| | AQUA | 50 % (0.114±0.075) | 35 % (0.079±0.070) | 15 % (0.034±0.023) | - |
| NAL | TERRA | 50 % (0.113±0.083) | 35 % (0.083±0.085) | 15 % (0.034±0.025) | - |
| | AQUA | 48 % (0.118±0.091) | 38 % (0.099±0.108) | 14 % (0.035±0.027) | - |
| BSO | TERRA | 53 % (0.108±0.103) | 22 % (0.044±0.101) | - | 25 % (0.051±0.016) |
| | AQUA | 51 % (0.094±0.087) | 22 % (0.042±0.085) | - | 27 % (0.051±0.016) |
| NWO | TERRA | 41 % (0.087±0.090) | 33 % (0.071±0.142) | - | 26 % (0.055±0.020) |
| | AQUA | 40 % (0.079±0.083) | 32 % (0.066±0.127) | - | 28 % (0.055±0.020) |
| SWO | TERRA | 32 % (0.071±0.070) | 42 % (0.097±0.257) | - | 26 % (0.058±0.018) |
| | AQUA | 32 % (0.093±0.288) | 41 % (0.072±0.080) | - | 27 % (0.059±0.018) |
| NEO | TERRA | 48 % (0.098±0.094) | 28 % (0.061±0.144) | - | 24 % (0.050±0.016) |
| | AQUA | 46 % (0.086±0.082) | 28 % (0.057±0.115) | - | 26 % (0.050±0.016) |
| SEO | TERRA | 36 % (0.079±0.070) | 39 % (0.087±0.224) | - | 25 % (0.055±0.016) |
| | AQUA | 36 % (0.075±0.071) | 38 % (0.080±0.217) | - | 26 % (0.055±0.016) |

10
 11
 12
 13
 14
 15
 16
 17
 18
 19
 20
 21
 22
 23

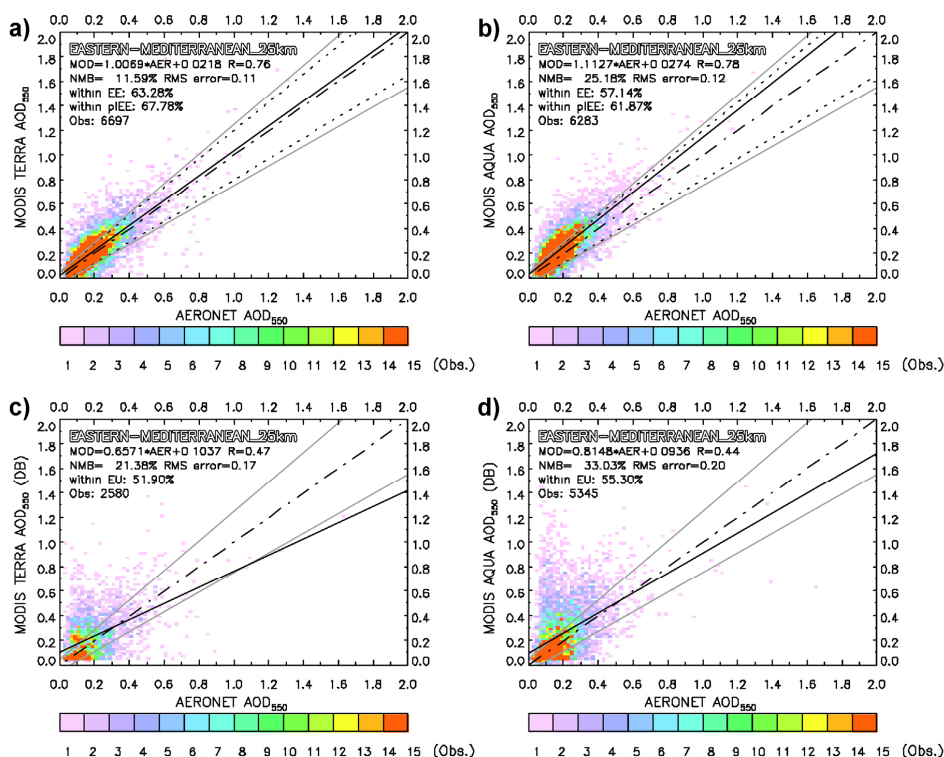


1
2 **Figure 1.** Eastern Mediterranean map with the 9 sub-regions selected for the generalization of
3 our results and the location of the AERONET stations used for the validation of MODIS
4 satellite data. The 9 sub-regions are: NBL (Northern Balkans Land), SBL (Southern Balkans
5 Land), ANL (Anatolia Land), NAL (Northern Africa Land), BSO (Black Sea Oceanic), NWO
6 (North-Western Oceanic), SWO (South-Western Oceanic), NEO (North-Eastern Oceanic) and
7 SEO (South-Eastern Oceanic). The full names and the geolocation of the 13 AERONET
8 stations appearing in the map are available in Table 1.



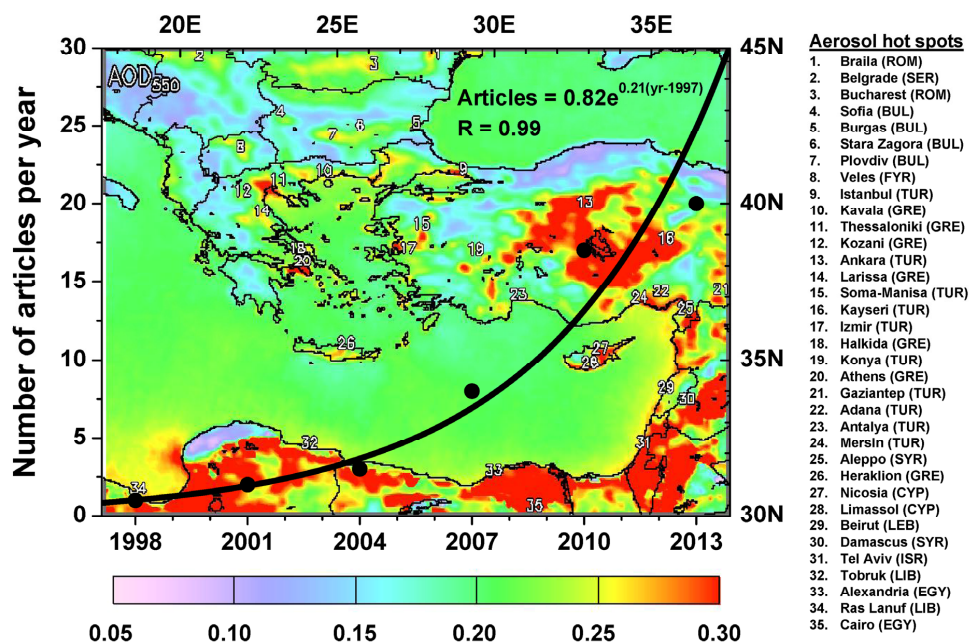
1
 2
 3
 4
 5
 6

Figure 2. Flowchart with the methodology followed for the calculation of the anthropogenic aerosol, dust and marine aerosol optical depths (τ_a , τ_d and τ_m) over the sea (blue color) and the anthropogenic aerosol, dust and fine mode natural aerosol optical depths (τ_a , τ_d and τ_n) over land (brown color).

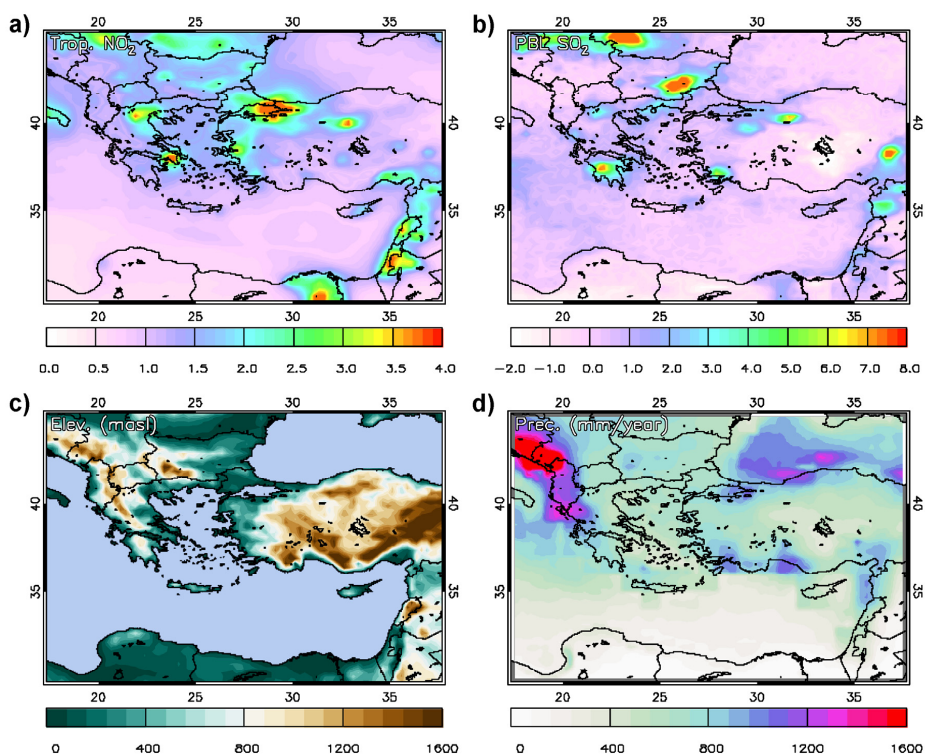


1
 2
 3
 4
 5
 6
 7
 8
 9
 10
 11
 12
 13
 14
 15
 16

Figure 3. Comparison of spatially (using a 25 x 25 km² window around each station) and temporally (± 30 min from the MODIS overpass time) collocated MODIS Collection 051 level-2 and AERONET sunphotometric (quadratically interpolated) AOD₅₅₀ observations for the Eastern Mediterranean stations: (a) for MODIS Terra DT data, (b) for MODIS Aqua DT data, (c) for MODIS Terra DB data and (d) for MODIS Aqua DB data. The color scale corresponds to the number of MODIS-AERONET collocation points that fall within 0.02 x 0.02 grid boxes. The solid line is the regression line of the MODIS-AERONET observations, the dashed-dotted line is the 1:1 line, the dotted lines represent the expected error (EE) envelope and the grey lines the pre-launch expected error (pLEE) envelope (Expected Uncertainty - EU envelope for DB data). The slope and the intercept of the regression line, the correlation coefficient R, the normalized mean bias (NMB), the root mean squared (RMS) error, the percentage of the collocation points that fall within the EE and pLEE and the number of all the collocation points.

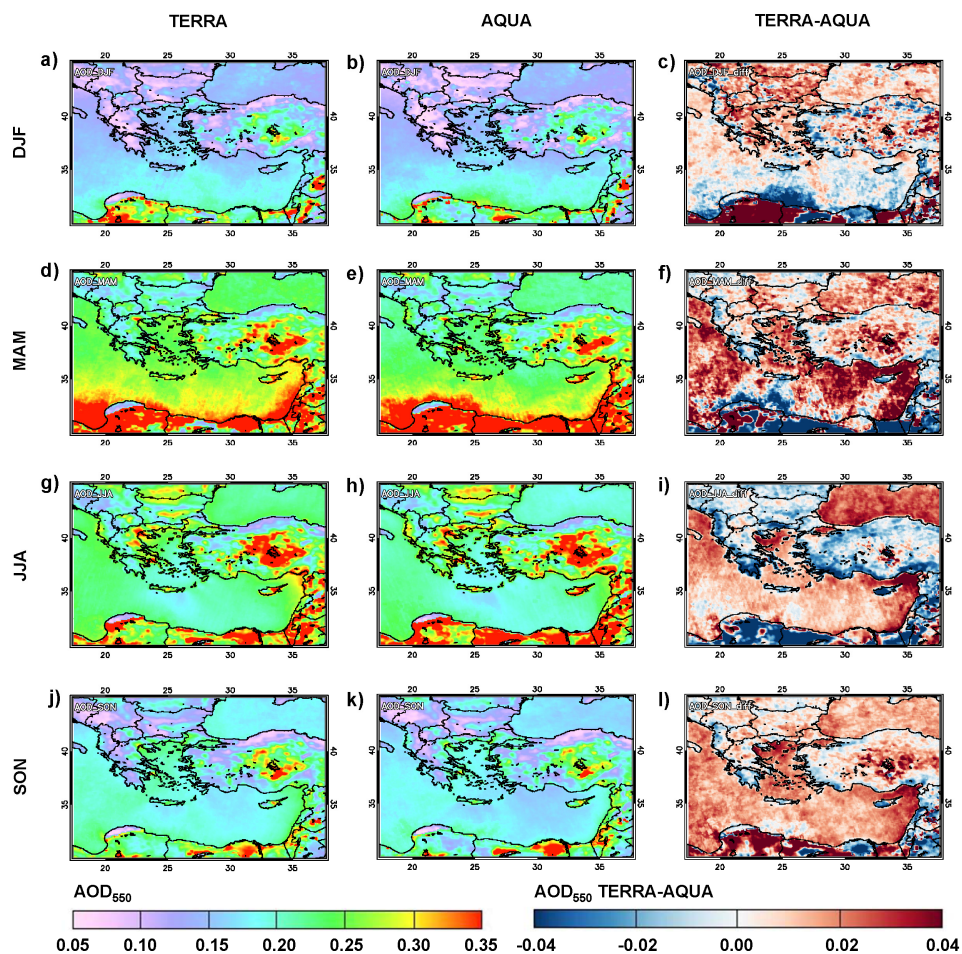


1
 2
 3 **Figure 4.** AOD₅₅₀ patterns over Eastern Mediterranean as seen by MODIS Terra during the
 4 period 3/2000-12/2012 (3/2000-12/2007 for regions of North Africa covered by DB data
 5 only). The colorscale corresponds to the AOD₅₅₀ levels while the top x-axis and the right y-
 6 axis correspond to the longitude (°E) and latitude (°N), respectively. The position of 35
 7 aerosol hot spots is marked on the map (numbers from 1 to 35) while the names of the places
 8 and the countries where the hot spots are located appear on the right of the map. In the same
 9 figure the exponential growth of the number of satellite-based articles focusing on aerosols
 10 over the greater Eastern Mediterranean from 1997 to 2014 is shown (black line). The black
 11 dots represent the number of articles published within three year intervals. The bottom x-axis
 12 and the left y-axis correspond to the years and the number of published articles, respectively.
 13 The exponential growth corresponds to a near doubling of the publication rate every 3 years.



1
2

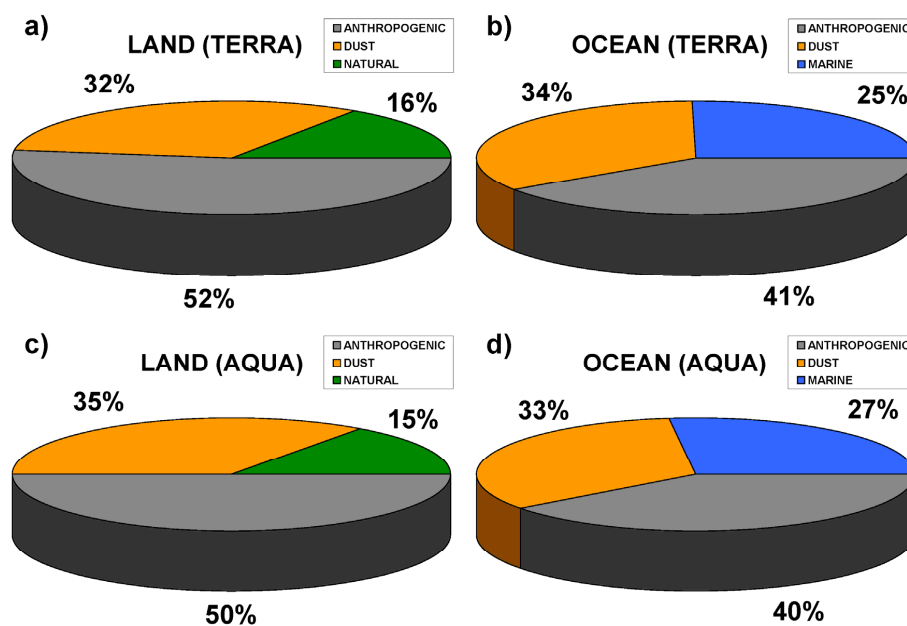
3 **Figure 5.** (a) Tropospheric NO₂ levels and (b) Planetary boundary layer SO₂ levels (in 10¹⁵
4 molecules/cm²) over the Eastern Mediterranean as seen from OMI/AURA (2005-2012), (c)
5 Topography (GTOPO elevation data in meters above sea level) and (d) Annual precipitation
6 levels (in mm/year) from 3B43 TRMM and Other Sources Monthly Rainfall Product (2000-
7 2012).



1

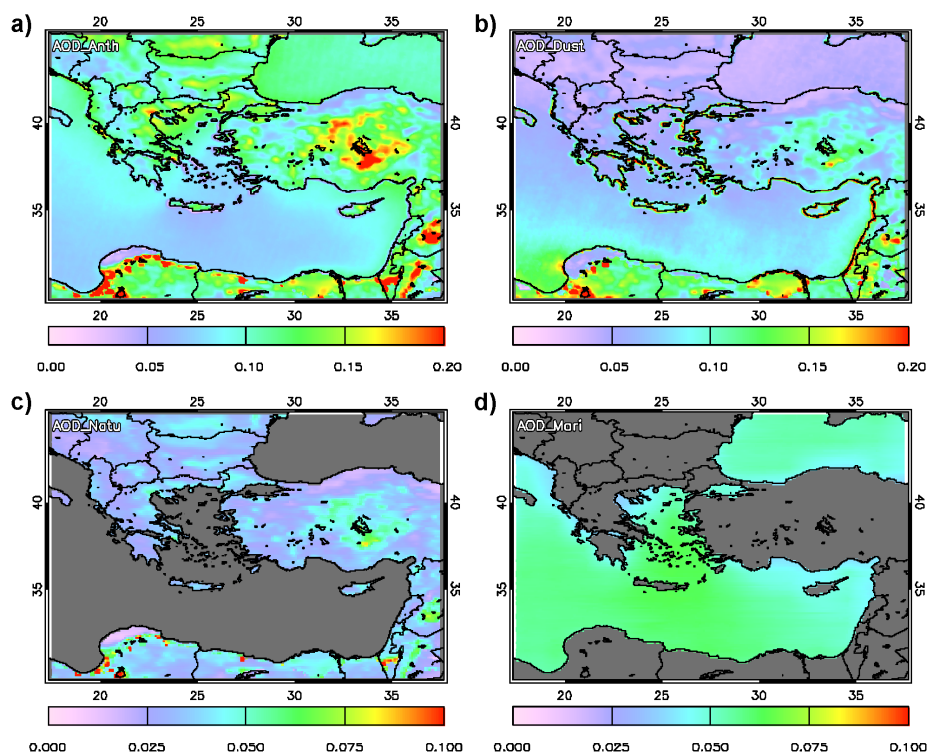
2

3 **Figure 6.** Seasonal AOD₅₅₀ patterns over the Eastern Mediterranean as seen by MODIS Terra
4 (left column) during the period 3/2000-12/2012 (3/2000-12/2007 for regions of North Africa
5 covered by DB data only) and MODIS Aqua (middle column) during the period 7/2002-
6 12/2012. The differences between MODIS Terra and Aqua AOD₅₅₀ on a seasonal basis appear
7 on the right column.



1
2

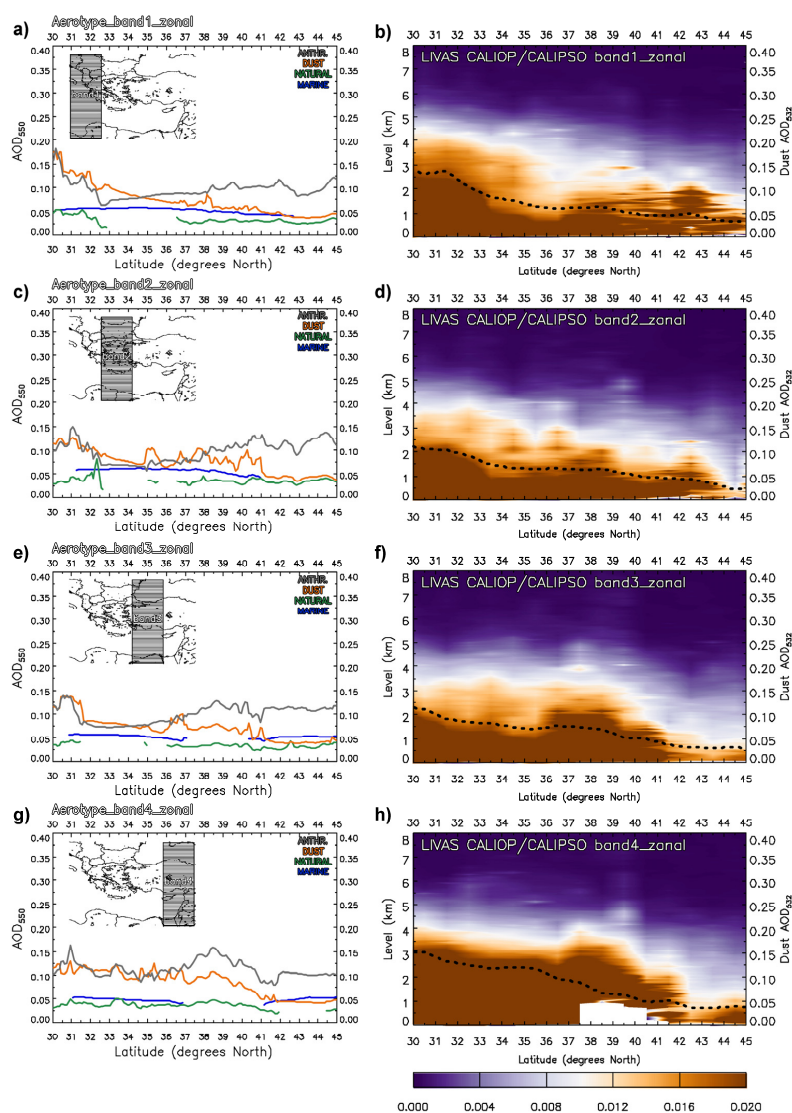
3 **Figure 7.** Relative contribution of anthropogenic aerosols, dust and fine mode natural
4 aerosols to the total AOD₅₅₀ over the land covered part of Eastern Mediterranean based on
5 MODIS Terra (a) and MODIS Aqua (c) observations and relative contribution of
6 anthropogenic aerosols, dust and marine aerosols to the total AOD₅₅₀ over the oceanic part of
7 Eastern Mediterranean based on MODIS Terra (b) and MODIS Aqua (d) observations.



1

2

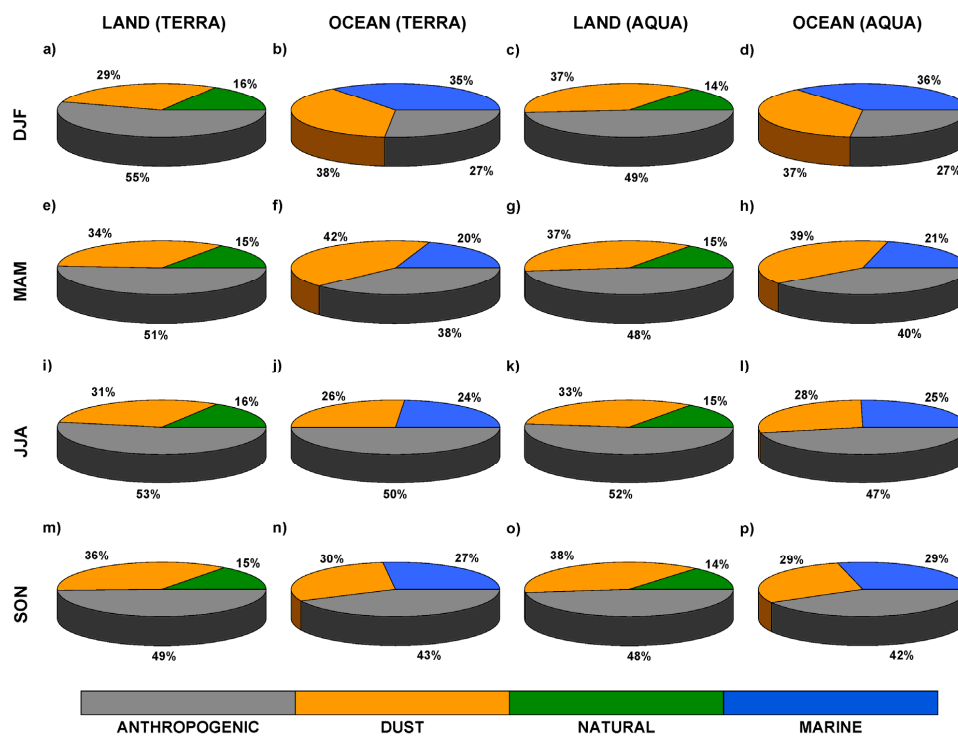
3 **Figure 8.** (a) Anthropogenic aerosol (τ_a), (b) dust (τ_d), (c) fine mode natural aerosol (τ_n) and
4 (d) marine aerosol (τ_m) patterns over the Eastern Mediterranean based on MODIS Terra
5 observations during the period 3/2000-12/2012 (3/2000-12/2007 for regions of North Africa
6 covered by DB data only).



1

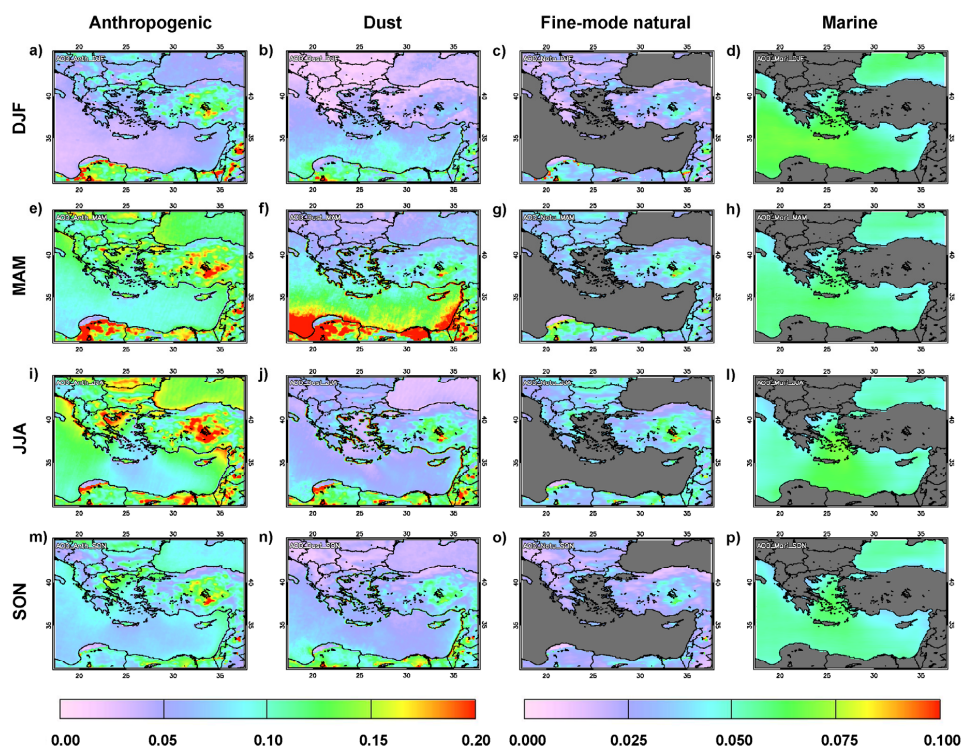
2

3 **Figure 9.** Left column: Latitudinal variability of anthropogenic aerosols (τ_a), dust (τ_d), fine
 4 mode natural aerosols (τ_n) and marine aerosols (τ_m) for four 5-degree longitudinal bands (see
 5 embedded maps) covering Eastern Mediterranean based on MODIS Terra observations. Right
 6 column: Latitudinal variability of dust extinction coefficients at 532 nm in km^{-1} (colorscale
 7 corresponds to the extinction coefficients and left y-axis to the atmospheric levels) and dust
 8 aerosol optical depth at 532 nm (dotted line corresponding to the right-y-axis) for the same
 9 four bands from LIVAS CALIOP/CALIPSO observations.



1
 2

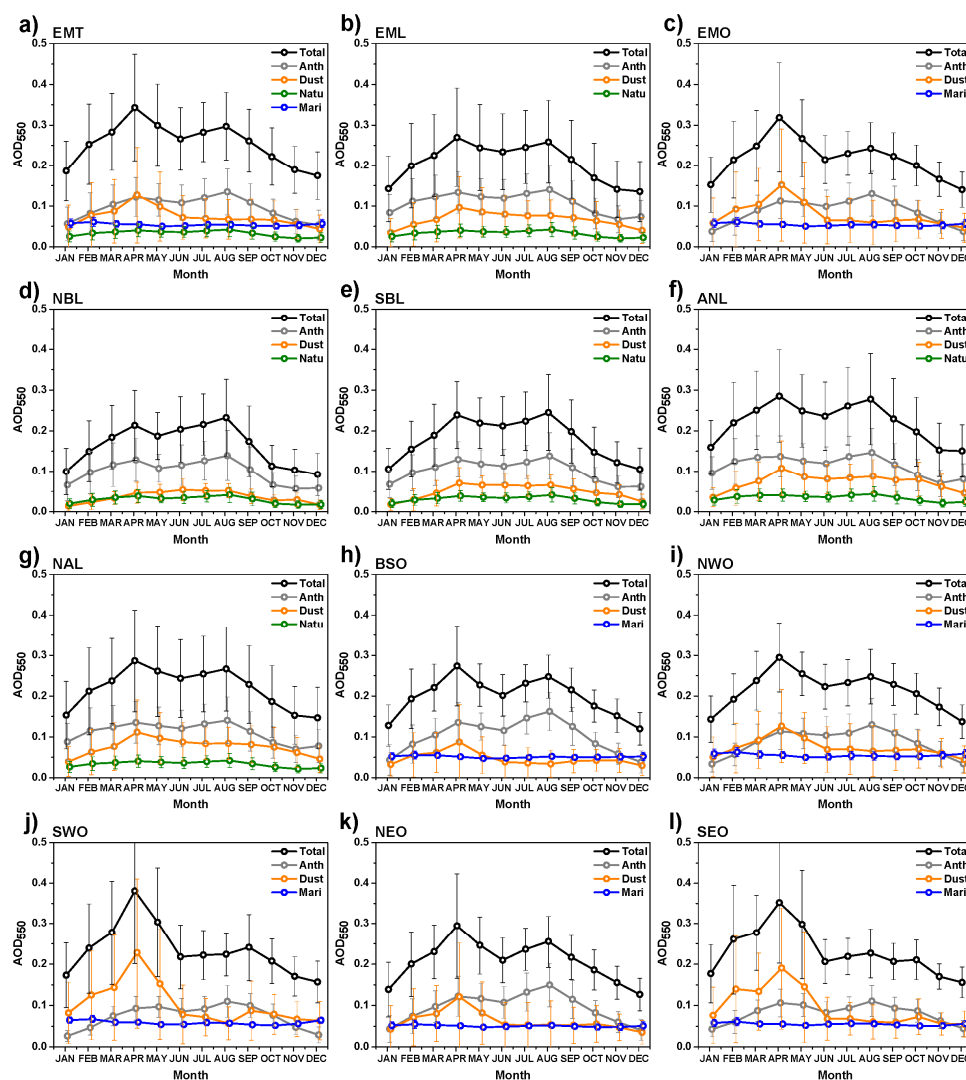
3 **Figure 10.** Seasonal relative contribution of anthropogenic aerosols, dust and fine mode
 4 natural aerosols to the total AOD₅₅₀ over the land covered part of Eastern Mediterranean
 5 based on MODIS Terra (a, e, i, m) and MODIS Aqua (c, g, k, o) observations and seasonal
 6 relative contribution of anthropogenic aerosols, dust and marine aerosols to the total AOD₅₅₀
 7 over the oceanic part of Eastern Mediterranean based on MODIS Terra (b, f, j, n) and MODIS
 8 Aqua (d, h, l, p) observations.



1

2

3 **Figure 11.** Seasonal (a, e, i, m) anthropogenic aerosol (τ_a), (b, f, j, n) dust (τ_d), (c, g, k, o) fine
4 mode natural aerosol (τ_n) and (d, h, i, p) marine aerosol (τ_m) patterns over the Eastern
5 Mediterranean based on MODIS Terra observations during the period 3/2000-12/2012
6 (3/2000-12/2007 for regions of North Africa covered by DB data only).



1

2

3 **Figure 12.** Seasonal variability of anthropogenic aerosols (τ_a), dust (τ_d), fine mode natural
 4 aerosols (τ_n) and marine aerosols (τ_m) over Eastern Mediterranean (EMT), over the land
 5 covered part (EML), over the oceanic part (EMO) and over the 9 sub-regions of the Eastern
 6 Mediterranean appearing in Fig. 1 based on MODIS Terra observations. The error bars
 7 represent the $\pm 1\sigma$ values calculated from monthly gridded data.